Mon. Not. R. Astron. Soc. **000**, 000–000 (0000) Printed 10 September 2012 (MN LATEX style file v2.2)

The clustering of galaxies in the SDSS-III Baryon Oscillation Spectroscopic Survey: constraints on the time variation of fundamental constants from the large-scale two-point correlation function

Claudia G. Scóccola[1,2⋆], Ariel G. Sánchez[3], J. A. Rubiño-Martín[1,2], R. Génova-Santos[1,2], R. Rebolo[1,2], A. J. Ross[4], W. J. Percival[4], M. Manera[4], D. Bizyaev[5], J. R. Brownstein[6], G. Ebelke[5], E. Malanushenko[5], V. Malanushenko[5], D. Oravetz[5], K. Pan[5], D. P. Schneider[7,8], A. Simmons[5]

[1] *Instituto de Astrofísica de Canarias (IAC), C/Vía Láctea, s/n, La Laguna, Tenerife, Spain.*
[2] *Dpto. Astrofísica, Universidad de La Laguna (ULL), E-38206 La Laguna, Tenerife, Spain.*
[3] *Max-Planck-Institut für extraterrestrische Physik, Postfach 1312, Giessenbachstr., 85748 Garching, Germany.*
[4] *Institute of Cosmology & Gravitation, University of Portsmouth, Dennis Sciama Building, Portsmouth PO1 3FX, UK.*
[5] *Apache Point Observatory, P.O. Box 59, Sunspot, NM 88349-0059, USA.*
[6] *Department of Physics and Astronomy, University of Utah, Salt Lake City, UT 84112, USA.*
[7] *Department of Astronomy and Astrophysics, Pennsylvania State University, University Park, PA 16802, USA.*
[8] *Institute for Gravitation and the Cosmos, The Pennsylvania State University, University Park, PA 16802, USA.*

Submitted to MNRAS

ABSTRACT

We obtain constraints on the variation of the fundamental constants from the full shape of the redshift-space correlation function of a sample of luminous galaxies drawn from the Data Release 9 of the Baryonic Oscillations Spectroscopic Survey. We combine this information with additional data from recent cosmic microwave background, baryon acoustic oscillations and H_0 measurements. We focus on possible variations of the fine structure constant α and the electron mass m_e in the early universe, and study the degeneracies between these constants and other cosmological parameters, such as the dark energy equation of state parameter $w_{\rm DE}$, the massive neutrinos fraction f_ν, the effective number of relativistic species $N_{\rm eff}$, and the primordial helium abundance $Y_{\rm He}$. In the case when only one of the fundamental constants is varied, our final bounds are $\alpha/\alpha_0 = 0.9957^{+0.0041}_{-0.0042}$ and $m_e/(m_e)_0 = 1.006^{+0.014}_{-0.013}$. For the joint variation of both fundamental constants, our results are $\alpha/\alpha_0 = 0.9901^{+0.0055}_{-0.0054}$ and $m_e/(m_e)_0 = 1.028 \pm 0.019$. The variations of α and m_e from their present values affects the bounds on other cosmological parameters. Although when m_e is allowed to vary our constraints on $w_{\rm DE}$ are consistent with a cosmological constant, when α is treated as a free parameter we find $w_{\rm DE} = -1.20 \pm 0.13$; more than 1 σ away from its standard value. When f_ν and α are allowed to vary simultaneously, we find $f_\nu < 0.043$ (95% CL), implying a limit of $\sum m_\nu < 0.46\,{\rm eV}$ (95% CL), while for m_e variation, we obtain $f_\nu < 0.086$ (95% CL), which implies $\sum m_\nu < 1.1\,{\rm eV}$ (95% CL). When $N_{\rm eff}$ or $Y_{\rm He}$ are considered as free parameters, their simultaneous variation with α provides constraints close to their standard values (when the H_0 prior is not included in the analysis), while when m_e is allowed to vary, their preferred values are significantly higher. In all cases, our results are consistent with no variations of α or m_e at the 1 or 2 σ level.

Key words: cosmological parameters, large-scale structure of Universe, early Universe

⋆ E-mail: scoccola@iac.es

1 INTRODUCTION

The overwhelming amount of cosmological observations obtained over the past few years has allowed not only the precise determination of the parameters of the standard cosmological model but also has provided plenty of scope to test non-standard physics and cosmological assumptions such as the constancy of fundamental constants over cosmological timescales.

The variation of fundamental constants is a prediction of theories attempting to unify the four interactions in nature, such as string derived field theories, related brane-world theories and Kaluza-Klein theories (see Uzan 2003; García-Berro et al. 2007, and references therein). Substantial work have been devoted to constrain such variations using cosmological observations (Rahmani et al. 2012; Coc et al. 2011; Levshakov et al. 2012; Menegoni et al. 2012; Landau & Scóccola 2010). Unifying theories predict the variation of all coupling constants, being all variations related in general to the rolling of a scalar field. In this paper we adopt a phenomenological approach and analyse the possible variation of the fine structure constant α and of the electron mass m_e between the recombination epoch and the present time, without assuming any theoretical model.

The cosmic microwave background (CMB) is a powerful tool to study the early universe. The acoustic oscillations present in the CMB power spectrum are also imprinted through the baryons on the large-scale structure (LSS) power spectrum (Eisenstein & Hu 1998; Meiksin et al. 1999). The correlation function $\xi(s)$ is the Fourier transform of the latter, and the oscillation structure appears there as a single peak whose position is related to the sound horizon at the drag redshift (Matsubara 2004). The ongoing Baryonic Oscillation Spectroscopic Survey (BOSS, Dawson et al. 2012) is a part of Sloan Digital Sky Survey-III (SDSS-III Eisenstein et al. 2011) and is aimed at obtaining redshifts for 1.5×10^6 massive galaxies out to $z = 0.7$ over an area of 10,000 deg^2. BOSS is designed to measure the baryon acoustic oscillations (BAO) signal to probe the expansion history of the universe. This information places complementary constraints on the variation of fundamental constants. A high redshift galaxy sample from BOSS Data Release 9 (DR9), denoted CMASS, is constructed through a set of colour-magnitude cuts designed to select a roughly volume-limited sample of massive, luminous galaxies (Eisenstein et al. 2011, Padmanabhan et al. in prep.). The clustering properties of the BOSS CMASS sample have been analysed in detail in a recent series of papers (Anderson et al. 2012; Manera et al. 2012; Reid et al. 2012; Ross et al. 2012; Samushia et al. 2012; Sánchez et al. 2012; Tojeiro et al. 2012).

The position of the peak in the correlation function of galaxies can place constraints on the variation of fundamental constants. Moreover, the full shape of the correlation function provides additional information that can break degeneracies, since some parameters vary the full shape, while others affect only the position and height of the BAO peak. We use the full shape of the correlation function of BOSS-CMASS galaxies presented in Sánchez et al. (2012), in combination with CMB observations, to place constraints on the time variation of fundamental constants in the early universe. We focus on possible variations in the fine structure constant, α, and the electron mass, m_e, at the recombination epoch. Strictly speaking, the acoustic fluctuations in the baryons are frozen in at the drag epoch rather than at last scattering (Hu & Sugiyama 1996). This dynamical decoupling of the baryons from the photons occurs nevertheless near recombination. Therefore, we assume that the values of the fundamental constants are the same throughout this epoch, though they can differ from their current values. We analyze the degeneracies with the basic cosmological parameters, as well as with others, such as the dark energy equation of state, the neutrino mass, the effective number of relativistic species, and the primordial helium abundance.

Limits on the present rate of variation of α and $\mu = m_e/m_p$ (where m_p is the proton mass) are provided by atomic clocks (Prestage et al. 1995; Sortais et al. 2001; Bize et al. 2003; Marion et al. 2003; Fischer et al. 2004; Peik et al. 2004). Data from the Oklo natural fission reactor (Damour & Dyson 1996; Fujii et al. 2000) and half-lives of long lived β decayers (Olive et al. 2004) allow to constrain the variation of fundamental constants at $z \simeq 1$. Absorption systems in the spectra of high-redshift quasars put additional constraints at different redshifts. The method is based on the measurement of the separation between spectral lines in doublets and multiplets, whose dependence on the constants vary among different species (see for example Webb et al. 1999, 2001; Murphy et al. 2003; Agafonova et al. 2011; Kanekar et al. 2012; Wendt & Molaro 2012). Although the limits imposed by CMB and LSS are less stringent than the previous ones, they are important because they refer to earlier times.

The paper is organized as follows. In Section 2 we show how the correlation function depends on the values of α and m_e at the recombination epoch. We describe the datasets used to place constraints on the variation of the fundamental constants and the statistical method performed. The modelling of the correlation function is also summarized. Section 3 presents the results for different parameter spaces. Conclusions are outlined in Section 4.

2 METHODOLOGY

We performed a statistical analysis to constrain the variation of α and m_e at the recombination epoch, together with other cosmological parameters varied. In this Section we describe the datasets used to obtain our results. Then, we summarize the modelling of the correlation function, and present a brief explanation of why the correlation function is an effective observable to constrain the variation of fundamental constants. Finally, we describe the statistical analysis employed.

2.1 Data

In this paper, we use the full shape of the large-scale two-point correlation function $\xi(s)$ of the BOSS-CMASS galaxy sample, computed in Sánchez et al. (2012). This function was computed using the first spectroscopic data release of BOSS (Data Release 9, DR9, SDSS-III Collaboration: Ahn et al. 2012). The galaxy target selection of BOSS is divided in two separate sam-

ples, named LOWZ and CMASS, covering different redshifts (Eisenstein et al. 2011; Padmanabhan et al. in prep.; Dawson et al. 2012). This selection is based on photometric observations done with the dedicated 2.5-m Sloan Telescope (Gunn et al. 2006), located at Apache Point Observatory in New Mexico, using a drift-scanning mosaic CCD camera (Gunn et al. 1998) that produces *ugriz* images (Fukugita et al. 1996). The CMASS sample is constructed on the basis of *gri* colour cuts designed to select luminous galaxies such that they constitute an approximately complete galaxy sample down to a limiting stellar mass (Maraston in prep.). Spectra of the LOWZ and CMASS samples are obtained using the double-armed BOSS spectrographs, which are significantly upgraded from those used by SDSS-I/II (York et al. 2000), covering the wavelength range 3600 Å to 10000 Å with a resolving power of 1500 to 2600 (Smee et al. 2012). Spectroscopic redshifts are measured using the minimum-χ^2 template-fitting procedure described in Aihara et al. (2011), with templates and methods updated for BOSS data as described in Bolton et al. (2012). Anderson et al. (2012) present a detailed description of the construction of the catalogue for LSS studies based on this sample, and the calculation of the completeness of each sector of the survey mask, i.e., the areas of the sky covered by a unique set of spectroscopic tiles.

To constrain high-dimensional parameter spaces, it is necessary to combine the CMASS $\xi(s)$ with other datasets. In our analysis, we use the WMAP 7-year temperature and temperature-polarization power spectra (Larson et al. 2011) and the results from the South Pole Telescope (SPT, Keisler et al. 2011). The latter provide information on the structure of the acoustic peaks in the CMB power spectrum up to multipoles $\ell \simeq 3000$. As discussed in Keisler et al. (2011), in the multipole range covered by SPT ($650 \leqslant \ell \leqslant 3000$), the CMB power spectrum contains a non-negligible contribution from secondary anisotropies, while for $\ell \lesssim 650$ the main contribution arises from primary anisotropies. We follow the approach of Keisler et al. (2011) to account for the secondary anisotropies, by including the contribution from the Sunyaev-Zel'dovich (SZ) effect and the emission from foreground galaxies (including both a clustered and a Poisson source contribution), using templates whose amplitudes are considered as nuisance parameters and marginalized over. The WMAP-SPT combination is referred to as our "CMB" dataset.

We also use information from other clustering measurements in the form of constraints on the position of the baryon acoustic peak from independent analyses. We use the results of Beutler et al. (2011) which are based on measurements of the large-scale correlation function of the 6dF Galaxy Survey (6DFGS, Jones et al. 2009) and the 2% distance measurement obtained by Padmanabhan et al. (2012) and Xu et al. (2012) from the application of an updated version of the reconstruction technique proposed by Eisenstein et al. (2007) to the clustering of galaxies from the final SDSS-II LRG sample (York et al. 2000; Eisenstein et al. 2011). The results of these analyses are combined in the "BAO" dataset.

Lastly, we consider a Gaussian prior on the Hubble parameter based on the latest Hubble Space Telescope (HST) observations of $\mathrm{H}_0 = 73.8 \pm 2.4\ \mathrm{km\,s^{-1}\,Mpc^{-1}}$ (Riess et al. 2011).

The aforementioned datasets are used in different combinations to check the consistency of the obtained bounds. Firstly, we use the CMB data alone, and then combine it with the CMASS correlation function. In the end, we combine the four datasets to obtain our final constraints.

We do not consider supernovae (SNs) type Ia data because the light curves of the SNs are obtained assuming that the fundamental constants have their present values at the observing redshift. However, since we are investigating a possible time evolution in the value of α and m_e, and the SNs are at considerably high redshift ($0.7 < z < 1.4$ for the high-z sample of Conley et al. 2011), we cannot neglect the possibility that the constants have a different value at those times. In fact, several studies aiming at measuring the value of α at high redshift using quasar absorption systems do not conclusively exclude the variation of fundamental constants at those redshifts (Webb et al. 1999, 2011; Murphy et al. 2003, 2004; King et al. 2012). Therefore, to be conservative, we choose not to consider the supernovae datasets in our analysis.

2.2 Model for the correlation function

We follow Sánchez et al. (2012) and model the shape of the large-scale correlation function, $\xi(s)$, by applying the following parametrization:

$$\xi(s) = b^2 \left[\xi_{\mathrm{L}}(s) \otimes \mathrm{e}^{-(k_\star s)^2} + A_{\mathrm{MC}}\, \xi'_{\mathrm{L}}(s)\, \xi^{(1)}_{\mathrm{L}}(s) \right], \qquad (1)$$

where the symbol $\otimes$ denotes a convolution, and the bias factor b, mode-coupling amplitude A_{MC}, and the smoothing length $k_\star$ are considered as free parameters and marginalized over. Here ξ'_{L} is the derivative of the linear correlation function ξ_{L}, and $\xi^{(1)}_{\mathrm{L}}(s)$ is defined by

$$\xi^{(1)}_{\mathrm{L}}(s) \equiv \hat{s} \cdot \nabla^{-1} \xi_{\mathrm{L}}(s) = \frac{1}{2\pi^2} \int P_{\mathrm{L}}(k)\, j_1(ks) k\, \mathrm{d}k, \qquad (2)$$

with $j_1(y)$ denoting the spherical Bessel function of order 1.

The parametrization of equation 1 was first proposed by Crocce & Scoccimarro (2008) and is based on renormalized perturbation theory (RPT, Crocce & Scoccimarro 2006). Sánchez et al. (2008) compared this model against the results of an ensemble of large volume N-body simulations (L-BASICC-II, Angulo et al. 2008), and showed that it provides an accurate description of the full shape of the correlation function, including also the effects of bias and redshift-space distortions. This parametrization has been applied to obtain constraints on cosmological parameters from clustering measurements from various galaxy samples (Sánchez et al. 2009; Beutler et al. 2011; Blake et al. 2011).

As in Sánchez et al. (2012), we restrict the comparison of the model of equation 1 and the BOSS-CMASS correlation function to $40 < s < 200\,h^{-1}\,\mathrm{Mpc}$, and assume a Gaussian likelihood function.

2.3 Effects on the full-shape of $\xi(s)$

During the recombination epoch, the ionization fraction is determined by the balance between photoionization and recombination. The most important effects of changes in α and m_e during this epoch are due to their influence upon Thomson scattering cross section $\sigma_T = 8\pi\hbar^2\alpha^2/3m_e^2c^2$ and

the binding energy of hydrogen $B_1 = \frac{1}{2}\alpha^2 m_e c^2$. The ionization history is more sensitive to α than to m_e because of the B_1 dependence on these constants. The main result is the shift of the epoch of recombination to higher z as α or m_e increases, which corresponds to a smaller sound horizon. These effects are imprinted into the matter power spectrum through the transfer function. Hence, they also affect the galaxy correlation function. Consequently, if at recombination α or m_e had a value higher than the present one, the peak in the correlation function would appear at smaller scales, since the position of the peak is related to the size of the sound horizon at the drag epoch.

Fig. 1 shows the effect of a variation in α and in m_e, during the recombination epoch, that we should expect in the correlation function of CMASS galaxies, in a flat universe with cosmological parameters $(\omega_{\rm b}, \omega_{\rm dm}, \tau, h, n_{\rm s}) = (0.0221, 0.1145, 0.696, 0.962)$. We show the prediction for different values of the fundamental constants: their present value, and a variation of $\pm 5\%$ with respect to their values today. Data points are the spherically averaged redshift-space two-point correlation function of the full CMASS sample presented in Sánchez et al. (2012).

The changes in the correlation function due to variations in α are larger than the changes in m_e for a given relative variation of their value. Both constants affect the position and height of the peak, leaving the rest of the curve unchanged. This effect can break degeneracies with other cosmological parameters that affect the full shape of the correlation function, such as the dark energy equation of state. Other parameters also affect the position of the peak. This leads to degeneracies between the fundamental constants and other cosmological parameters, such as $\Omega_{\rm m}$, as we will see in Sections 3.1 and 3.2. The combination of CMASS data with different datasets helps to break those degeneracies.

2.4 Statistical Analysis

We perform our statistical analysis by exploring the parameter spaces with Monte Carlo Markov chains generated with the CosmoMC code (Lewis & Bridle 2002), which uses the Boltzmann code CAMB (Lewis et al. 2000) and RECFAST (Seager et al. 1999) to compute the CMB power spectra. In order to be able to study more general models in which the dark energy component is different from the cosmological constant, we use a generalized version of CAMB which supports values of the dark energy equation of state beyond the phantom divide, $w_{\rm DE} < -1$ (Fang et al. 2008). We modified these codes to include the variation in α and m_e at recombination as described in Landau et al. (2008). Additional modifications from Keisler et al. (2011) are included to compute the likelihood of the SPT dataset. The dependence on the fundamental constants of the detailed physics relevant in the recombination process is described in Scóccola et al. (2008). Nevertheless, we emphasize that such description is done in terms of a modification to the effective 3-level atom model which is used in RECFAST (Wong et al. 2008). Additional physical processes (see e.g., Rubiño-Martín et al. 2008; Fendt et al. 2009, for a review) are effectively treated using a correction function inside RECFAST v1.5 (Rubiño-Martín et al. 2010). This function has, to first order, a negligible dependence on the standard

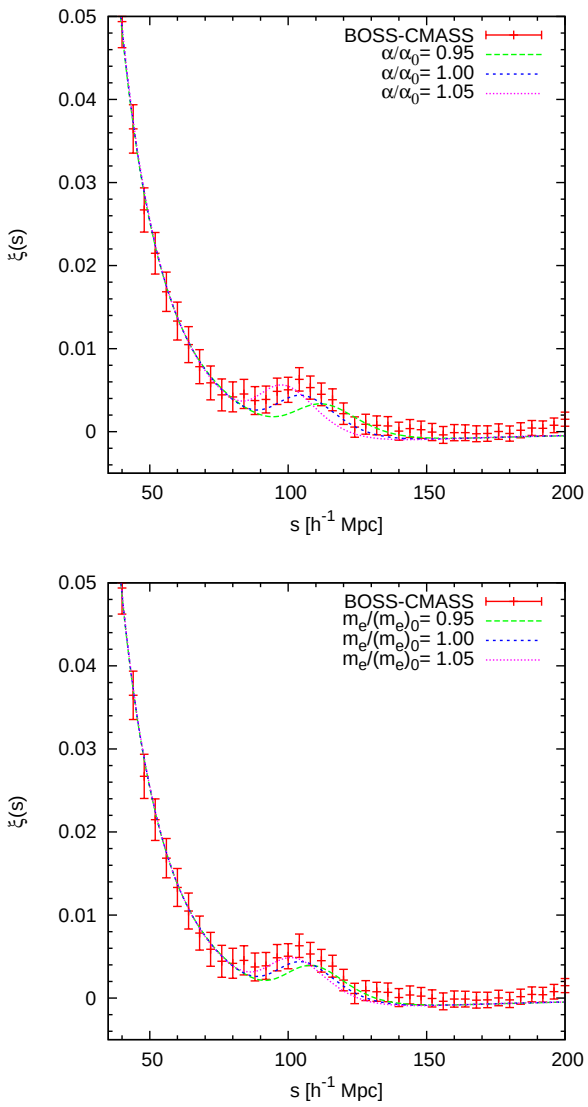

Figure 1. Effects on the two-point correlation function of a 5% variation in α (upper panel), and in m_e (lower panel) at recombination time, with respect to their present values. Other parameters are kept fixed

. Data points are the measurement of the BOSS-CMASS two-point correlation function from Sánchez et al. (2012).

cosmological parameters, but also on non-standard parameters such as $Y_{\rm He}$ or $N_{\rm eff}$ (Shaw & Chluba 2011). Although it has not been demonstrated explicitly, this correction function is also expected to have a small dependence on α and m_e. Thus, we will use in this paper the correction function as it appears in RECFAST v1.5. However, for future CMB experiments with higher sensitivities in the damping tail of the angular power spectrum, a more detailed and complete treatment of the recombination problem might be relevant (Chluba & Thomas 2011).

We consider a spatially-flat cosmological model with adiabatic density fluctuations, described by the following parameters, which define the ΛCDM model:

$$P = (\omega_{\rm b}, \omega_{\rm dm}, \Theta, \tau, A_{\rm s}, n_{\rm s}) \quad (3)$$

where $\omega_{\rm b} = \Omega_{\rm b} h^2$ is the baryon density, $\omega_{\rm dm} = \Omega_{\rm dm} h^2$ is the

dark matter density, both in units of the critical density; Θ gives the ratio of the comoving sound horizon at decoupling to the angular diameter distance to the surface of last scattering; τ is the reionization optical depth; and $A_{\rm s}$ and $n_{\rm s}$ are the amplitude and spectral index of the primordial power spectrum of the scalar fluctuations, respectively, at the pivot wavenumber of $k = 0.05\,{\rm Mpc}^{-1}$.

To this set of cosmological parameters, we add the value of α and/or m_e at the recombination epoch as additional variables. We introduce them as α/α_0 and $m_e/(m_e)_0$, i.e., relative to their present value, denoted with a 0 subscript.

Moreover, to constrain possible deviations from the ΛCDM model, we study also the cases in which we allow for variations of the dark energy equation of state $w_{\rm DE}$ and the dark matter fraction in the form of massive neutrinos, $f_\nu = \Omega_\nu/\Omega_{\rm dm}$, focusing on the degeneracies with the fundamental constants studied here. In addition, we analyze the case in which the effective number of relativistic species is different from its standard value of $N_{\rm eff} = 3.046$, and the case in which the primordial helium fraction can have a value different than the standard one of $Y_{\rm He} = 0.24$. Finally, we present the constraints on the parameters of the ΛCDM+$N_{\rm eff}$ and ΛCDM+$Y_{\rm He}$ models in the case of no variation of the fundamental constants.

We also present constraints on other quantities, derived from the above parameter set. These are the sum of the neutrino masses, given by

$$\sum m_\nu = 94.4\,\omega_{\rm dm}\,f_\nu\ {\rm eV}, \qquad (4)$$

the dark energy density $\Omega_{\rm DE}$, the total matter density $\Omega_{\rm m}$, the rms linear perturbation theory variance in spheres of radius $8\,h^{-1}$Mpc σ_8, the age of the universe t_0, the redshift of reionization $z_{\rm re}$, and the hubble factor h.

The parameters b, $A_{\rm MC}$, and $k_\star$ of the model for the full shape of the correlation function, and the amplitudes $D^{\rm SZ}_{3000}$, $D^{\rm PS}_{3000}$, $D^{\rm CL}_{3000}$, necessary to account for the secondary anisotropies in the SPT power spectrum, are treated as nuisance parameters, and marginalized over when presenting our results.

For most of the cases, we only use the information from the CMASS correlation function in combination with our CMB data. However, in Sections 3.1 and 3.2, we also ran chains using the CMASS information alone, to study the degeneracies between α and m_e and other cosmological parameters obtained from this dataset. In these cases we impose Gaussian priors on $\omega_{\rm b}$ and $n_{\rm s}$, obtained from CMB-only results (see first column of Table 1 and Table 2).

3 RESULTS

We present the constraints obtained for the fundamental constants and cosmological parameters in each of the cases studied. Errorbars will indicate 68% confidence level (CL) unless otherwise stated. In Section 3.1 we study the variation of the fine structure constant, and do the statistical analysis varying also the cosmological parameters of the ΛCDM model. In Section 3.2 we study the variation of the electron mass together with the cosmological parameters. Section 3.3 investigates the joint variation of α and m_e. In Section 3.4 we analyze the constraints in the case where one of the constants (α or m_e) and the dark energy equation of state $w_{\rm DE}$ can take values that differ from the standard ones. In Section 3.5 we study the case where we vary one of the fundamental constants and the massive neutrinos fraction f_ν. Section 3.6 focusses on the constraints obtained when the fundamental constants are varied together with the effective number of relativistic species, $N_{\rm eff}$, while Section 3.7 presents the constraints when the fundamental constants are varied together with the primordial helium fraction $Y_{\rm He}$. In Appendix A, we give the constraints on the ΛCDM model for our four datasets, to facilitate the comparison to the results presented in this paper.

3.1 Variation of α

In this Section, we extend the ΛCDM model to include possible variations in the fine structure constant during recombination. We present our constraints on α/α_0 and the cosmological parameters.

The upper panel of Fig. 2 shows the two-dimensional marginalized constraints in the α - $\Omega_{\rm m}$ plane obtained from the CMB and CMASS datasets in isolation. As specified in Section 2, when using the information of the CMASS correlation function alone we impose Gaussian priors on $\omega_{\rm b}$ and $n_{\rm s}$ consistent with our CMB-only results. The constraints obtained from these datasets exhibit strong degeneracies. As these degeneracies constrain different combinations of α and $\Omega_{\rm m}$, the combination of the two datasets provides tighter constraints on both parameters simultaneously. As can seen in the lower panel of Fig. 2, the remaining degeneracy between these parameters is alleviated when more datasets are added to the analysis. The correlation factors are -0.62, -0.38, and -0.13 for CMB, CMB+CMASS, and the full dataset combination (CMB+CMASS+BAO+H_0), respectively.

In Fig. 3 we show the constraints in the α - H_0 plane. H_0 is better constrained when additional datasets are included in the analysis. The value of the HST prior on H_0 lies almost $2\,\sigma$ from the value obtained for H_0 from the CMB+CMASS dataset, being the latter considerably smaller. Hence, when the HST prior on H_0 is taken into account, the obtained value for the Hubble parameter is increased. Due to the degeneracy with α, the contours are shifted in the parameter space when the H_0 prior is included, and the value of the fine structure constant is increased, being closer to its present value.

In Table 1 we present the constraints on the variation of α and the cosmological parameters. The constraint on α from CMB data alone is $\alpha/\alpha_0 = 0.9914 \pm 0.0055$. The CMB-only constraints on $\Omega_{\rm m}$ are considerably degraded by the inclusion of α as a free parameter, with $\Omega_{\rm m} = 0.303^{+0.037}_{-0.036}$ (compare to the ΛCDM value of $\Omega_{\rm m}$ in Table A1 of the Appendix). When we add the information encoded in the full shape of the CMASS $\xi(s)$, we find $\alpha/\alpha_0 = 0.9917 \pm 0.0046$ and $\Omega_{\rm m} = 0.295^{+0.017}_{-0.018}$. In the case that all datasets are used in the analysis, the constraints are $\alpha = 0.9957^{+0.0041}_{-0.0042}$ and $\Omega_{\rm m} = 0.283 \pm 0.010$, which is the same precision as that obtained in the ΛCDM model. The inclusion of the additional datasets produces only a mild improvement of the bounds on α with respect to those obtained using CMB information alone. This result arises because our CMB dataset covers the high multipole range, with $\ell \sim 3000$, which imposes strong constraints on this parameter. The bounds obtained for the

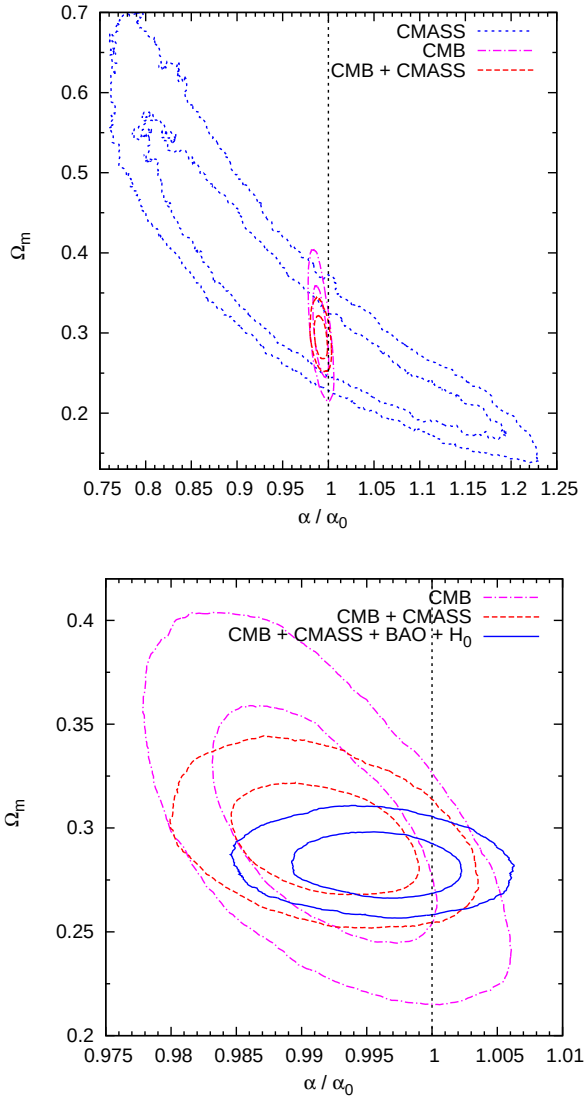

Figure 2. The marginalized posterior distribution in the α - $\Omega_{\rm m}$ plane for the ΛCDM parameter set extended to include the variation of α. The dot-dashed lines show the 68% and 95% contours obtained using CMB information alone. The dotted contours, in the upper panel, show the results from CMASS correlation function. The dashed lines correspond to the results obtained from the combination of CMB data plus the shape of the CMASS $\xi(s)$. The solid lines indicate the results obtained from the full dataset combination (CMB+CMASS+BAO+H_0). The vertical dotted line corresponds to the ΛCDM model, with $\alpha/\alpha_0 = 1$

.

cosmological parameters from the full dataset are consistent within 1 σ with their values in the ΛCDM model (see Table A1).

Menegoni et al. (2012) present constraints on the variation of α using CMB data including data from SPT and the Atacama Cosmology Telescope (ACT, Dunkley et al. 2011), both probing the damping regime of the CMB fluctuations. By combining this information with the galaxy power spectrum from the SDSS-DR7 luminous red galaxy sample (Reid et al. 2010) and the HST prior on H_0, they find $\alpha/\alpha_0 = 0.984 \pm 0.005$. The precision on this constraint on α

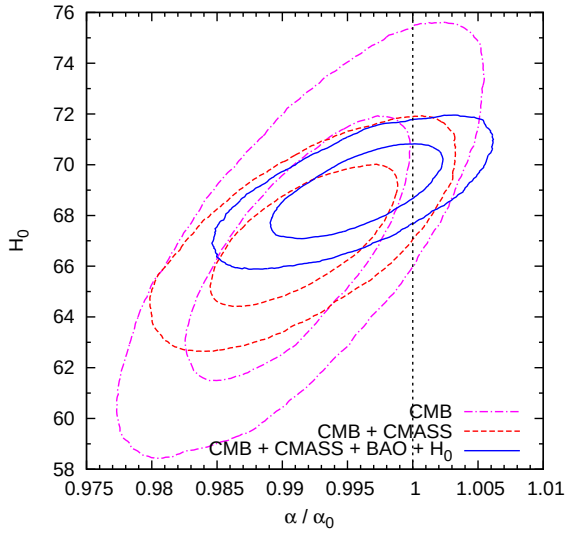

Figure 3. The marginalized posterior distribution in the α - H_0 plane for the ΛCDM parameter set extended to include the variation of α. The dot-dashed lines show the 68% and 95% contours obtained using CMB information alone. The dashed lines correspond to the results obtained from the combination of CMB data plus the shape of the CMASS $\xi(s)$. The solid lines indicate the results obtained from the full dataset combination (CMB+CMASS+BAO+H_0).

is provided mostly by the CMB data, explaining why our results with CMB data alone have almost the same precision as theirs. Nevertheless, the CMASS $\xi(s)$ further improves the precision of the bound. It is important to emphasize, however, that our results prefer values for α that are closer to its present value than theirs. Our results are consistent with no variation of α at 2 σ (for the full dataset, they are just slightly inconsistent at 1 σ).

3.2 Variation of m_e

Now we turn to the case in which we extend the ΛCDM model to include possible variations in the electron mass during recombination.

The contours in Fig. 4 show the two-dimensional marginalized constraints in the m_e - $\Omega_{\rm m}$ plane. The upper panel shows that the constraints obtained from the CMB and CMASS datasets in isolation exhibit strong degeneracies in different directions in the parameter space. The CMB-only constraints exhibit a strong degeneracy between m_e and $\Omega_{\rm m}$, causing $\Omega_{\rm m}$ to be poorly constrained by the CMB data alone, with $\Omega_{\rm m} = 0.31^{+0.12}_{-0.11}$. The inclusion of the CMASS correlation function improves the constraints on $\Omega_{\rm m}$ by a factor larger than five to obtain $\Omega_{\rm m} = 0.295 \pm 0.021$. This bound is further reduced by a factor of two when all datasets are included, in which case we find $\Omega_{\rm m} = 0.280 \pm 0.010$, having the same precision than in the ΛCDM model.

In Fig. 5 we show the two-dimensional marginalized constraints in the m_e - H_0 plane. When m_e is allowed to vary, CMB information alone is insufficient to place any reliable constraint on H_0. When the CMASS dataset is added, the constraint improves noticeably. This dataset breaks the degeneracy between H_0 and m_e. When all the datasets are

Table 1. The marginalized 68% allowed regions on the cosmological parameters of the ΛCDM model, adding the variation of the fine structure constant, α, obtained using different combinations of the datasets.

	CMB	CMB + CMASS	CMB + CMASS + BAO + H_0
α/α_0	$0.9914^{+0.0055}_{-0.0055}$	$0.9917^{+0.0046}_{-0.0046}$	$0.9957^{+0.0041}_{-0.0042}$
100Θ	$1.0289^{+0.0078}_{-0.0078}$	$1.0293^{+0.0064}_{-0.0065}$	$1.0353^{+0.0057}_{-0.0058}$
$100\omega_{\rm b}$	$2.207^{+0.043}_{-0.043}$	$2.209^{+0.039}_{-0.039}$	$2.225^{+0.038}_{-0.039}$
$100\omega_{\rm dm}$	$11.17^{+0.48}_{-0.47}$	$11.09^{+0.36}_{-0.36}$	$11.19^{+0.33}_{-0.34}$
τ	$0.0880^{+0.0064}_{-0.0073}$	$0.0877^{+0.0064}_{-0.0072}$	$0.0867^{+0.0061}_{-0.0072}$
$n_{\rm s}$	$0.977^{+0.013}_{-0.013}$	$0.977^{+0.013}_{-0.013}$	$0.973^{+0.013}_{-0.013}$
$\ln(10^{10}A_{\rm s})$	$3.104^{+0.034}_{-0.034}$	$3.101^{+0.032}_{-0.031}$	$3.095^{+0.030}_{-0.030}$
$\Omega_{\rm DE}$	$0.697^{+0.036}_{-0.037}$	$0.705^{+0.018}_{-0.017}$	$0.717^{+0.010}_{-0.010}$
$\Omega_{\rm m}$	$0.303^{+0.037}_{-0.036}$	$0.295^{+0.017}_{-0.018}$	$0.283^{+0.010}_{-0.010}$
σ_8	$0.815^{+0.023}_{-0.023}$	$0.813^{+0.020}_{-0.020}$	$0.818^{+0.018}_{-0.018}$
t_0/Gyr	$14.12^{+0.26}_{-0.26}$	$14.10^{+0.20}_{-0.19}$	$13.90^{+0.17}_{-0.16}$
$z_{\rm re}$	$10.8^{+1.2}_{-1.2}$	$10.8^{+1.2}_{-1.2}$	$10.6^{+1.2}_{-1.2}$
h	$0.668^{+0.033}_{-0.033}$	$0.672^{+0.018}_{-0.018}$	$0.689^{+0.012}_{-0.012}$

considered, the value of H_0 is increased due to the HST prior, and the value of m_e is shifted towards its present value.

In Table 2 we present the constraints on the variation of m_e and the cosmological parameters. The constraint on m_e from CMB data alone is $0.989^{+0.067}_{-0.069}$. When we add the information encoded in the full shape of the CMASS $\xi(s)$, the bound is $0.981^{+0.020}_{-0.021}$. In the case that all datasets are used in the analysis, the constraint is $1.006^{+0.014}_{-0.013}$. The precision in the bound is highly improved when we add the information of the CMASS $\xi(s)$ to the analysis. Our final results are completely consistent with no variation of m_e within 1 σ.

The bounds for the cosmological parameters are consistent within 1 σ with those from the ΛCDM model. The mean values of σ_8 and h for the CMB+CMASS dataset are somewhat smaller than in the ΛCDM model, but still consistent within 1 σ.

3.3 Joint variation of α and m_e

In this Section, we extend the ΛCDM model to study the joint variation of α and m_e.

The contours in Fig. 6 show the two-dimensional marginalized constraints in the m_e - α plane. When the H_0 prior is used, the mean value of α is marginally decreased, while the mean value of m_e is increased. The inclusion of additional datasets reduces the allowed region in the parameter space, while increasing the correlation between the fundamental constants; the correlation factor is −0.23, −0.55, and −0.68 for CMB, CMB+CMASS, and the full dataset combination (CMB+CMASS+BAO+H_0), respectively.

In Table 3 we present the constraints obtained for the fundamental constants and the cosmological parameters. When adding different datasets, the precision in the determination of α remains the same, although the mean value is slightly lower when the full dataset is used. For the CMB and CMB+CMASS datasets, the mean value of α is almost the same, regardless of m_e being fixed to its present value or allowed to vary. For the full dataset, the value of α is decreased by 1 σ when m_e is also allowed to vary (see Fig. 7).

The constraints on m_e are significantly improved when adding extra datasets. The bound on m_e from CMB-only data is improved by almost a factor of three when the CMASS dataset is added to the analysis, and is further improved when all the datasets are considered. The mean value of m_e is increased when α is also allowed to vary, compared to the case in which α is fixed to its present value. For

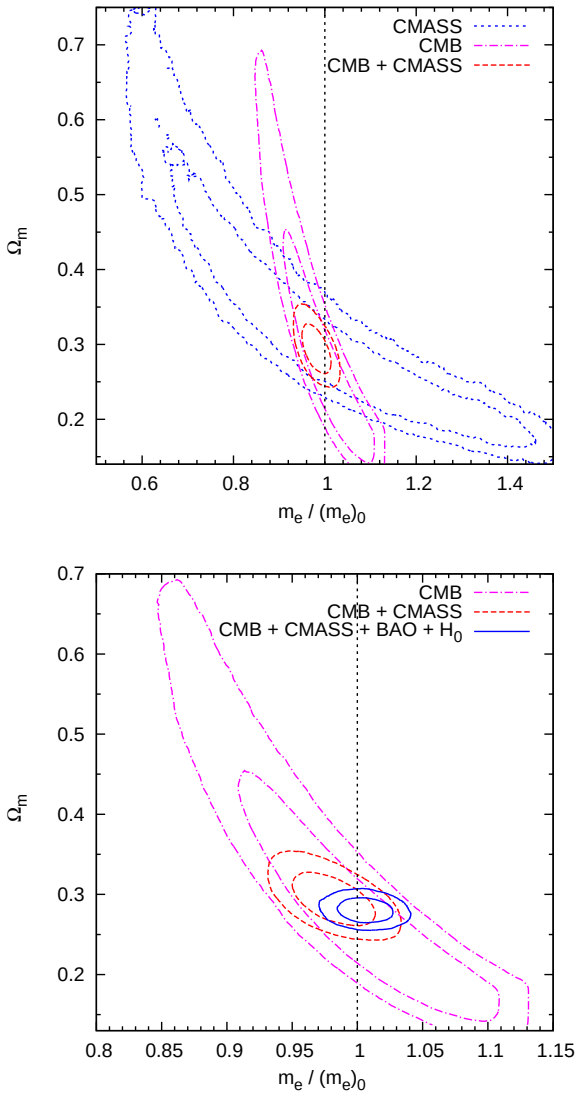

Figure 4. The marginalized posterior distribution in the m_e - $\Omega_{\rm m}$ plane for the ΛCDM parameter set extended to include the variation of m_e. The dot-dashed lines show the 68% and 95% contours obtained using CMB information alone. The dotted contours, in the upper panel, show the results from CMASS correlation function.

The dashed lines correspond to the results obtained from the combination of CMB data plus the shape of the CMASS $\xi(s)$. The solid lines indicate the results obtained from the full dataset combination (CMB+CMASS+BAO+H_0). The vertical dotted line corresponds to the ΛCDM model, with $m_e/(m_e)_0 = 1$.

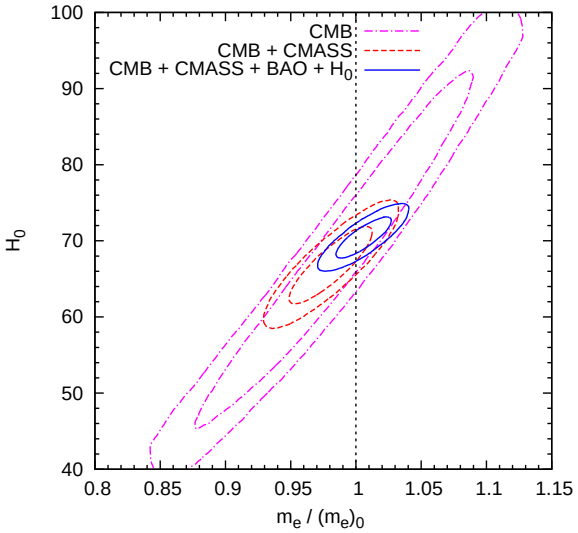

Figure 5. The marginalized posterior distribution in the m_e - H_0 plane for the ΛCDM parameter set extended to include the variation of $m_e/(m_e)_0$. The dot-dashed lines show the 68% and 95% contours obtained using CMB information alone. The dashed lines correspond to the results obtained from the combination of CMB data plus the shape of the CMASS $\xi(s)$. The solid lines indicate the results obtained from the full dataset combination (CMB+CMASS+BAO+H_0).

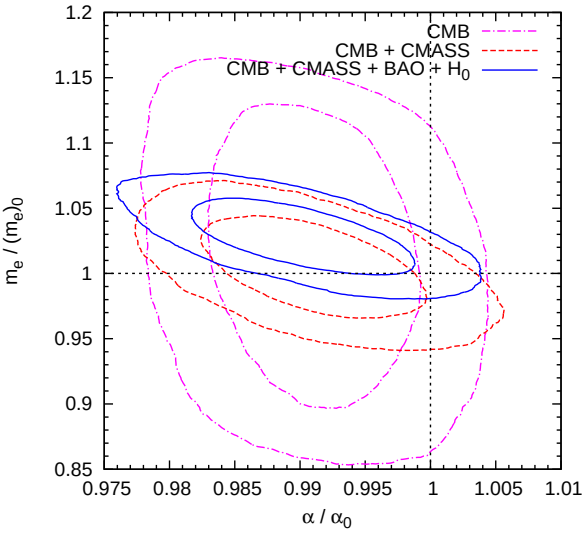

Figure 6. The marginalized posterior distribution in the α - m_e plane for the ΛCDM parameter set extended to include the joint variation of α and m_e. The dot-dashed lines show the 68% and 95% contours obtained using CMB information alone. The dashed lines correspond to the results obtained from the combination of CMB data plus the shape of the CMASS $\xi(s)$. The solid lines indicate the results obtained from the full dataset combination (CMB+CMASS+BAO+H_0).

Table 2. The marginalized 68% allowed regions on the cosmological parameters of the ΛCDM model, adding the variation of the electron mass, m_e, obtained using different combinations of the datasets.

	CMB	CMB + CMASS	CMB + CMASS + BAO + H_0
$m_e/(m_e)_0$	$0.989^{+0.067}_{-0.069}$	$0.981^{+0.020}_{-0.021}$	$1.006^{+0.014}_{-0.013}$
100Θ	$1.033^{+0.049}_{-0.051}$	$1.027^{+0.015}_{-0.015}$	$1.0448^{+0.0097}_{-0.0094}$
$100\omega_{\rm b}$	$2.20^{+0.17}_{-0.17}$	$2.177^{+0.054}_{-0.054}$	$2.228^{+0.042}_{-0.042}$
$100\omega_{\rm dm}$	$11.06^{+0.87}_{-0.88}$	$10.95^{+0.63}_{-0.64}$	$11.67^{+0.55}_{-0.54}$
τ	$0.0850^{+0.0063}_{-0.0071}$	$0.0850^{+0.0061}_{-0.0069}$	$0.0813^{+0.0059}_{-0.0066}$
$n_{\rm s}$	$0.965^{+0.012}_{-0.012}$	$0.9646^{+0.0100}_{-0.0099}$	$0.9620^{+0.0098}_{-0.0098}$
$\ln(10^{10}A_{\rm s})$	$3.080^{+0.031}_{-0.031}$	$3.078^{+0.031}_{-0.030}$	$3.089^{+0.029}_{-0.029}$
$\Omega_{\rm DE}$	$0.69^{+0.11}_{-0.12}$	$0.705^{+0.021}_{-0.021}$	$0.720^{+0.010}_{-0.010}$
$\Omega_{\rm m}$	$0.31^{+0.12}_{-0.11}$	$0.295^{+0.021}_{-0.021}$	$0.280^{+0.010}_{-0.010}$
σ_8	$0.799^{+0.072}_{-0.074}$	$0.794^{+0.039}_{-0.039}$	$0.839^{+0.032}_{-0.031}$
t_0/Gyr	$14.1^{+1.7}_{-1.6}$	$14.20^{+0.47}_{-0.47}$	$13.64^{+0.28}_{-0.28}$
$z_{\rm re}$	$10.3^{+1.4}_{-1.4}$	$10.2^{+1.1}_{-1.1}$	$10.3^{+1.2}_{-1.2}$
h	$0.69^{+0.15}_{-0.15}$	$0.668^{+0.032}_{-0.032}$	$0.704^{+0.017}_{-0.017}$

the CMB+CMASS and the full datasets, the increment is more than 1 σ (see Fig. 8 for the full dataset case). For the full dataset combination, the mean value of m_e takes its largest value. Our final bounds, using the full dataset, are $\alpha/\alpha_0 = 0.9901^{+0.0055}_{-0.0054}$ and $m_e/(m_e)_0 = 1.028^{+0.019}_{-0.019}$. Both

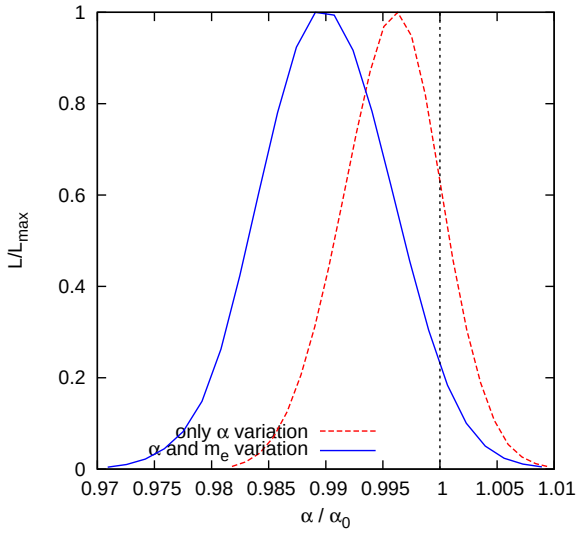

Figure 7. The marginalized, one-dimensional likelihood distribution for the fine structure constant, when only α is allowed to vary, and in the case of the joint variation of α and m_e.

limits are consistent with no variation of the fundamental constants at the 2 σ level.

Most of the cosmological parameters are consistent within 1 σ with their ΛCDM model values for each of the datasets. The value of $n_{\rm s}$ is larger than in the ΛCDM model, for all of the datasets. For the CMB+CMASS and the full datasets, $n_{\rm s}$ is larger by slightly more than 1 σ. The value of σ_8 is slightly larger than its value in the ΛCDM model, but consistent within 1 σ.

Table 3. The marginalized 68% allowed regions on the cosmological parameters of the ΛCDM model, adding the variation of the fine structure constant α and of the electron mass m_e, obtained using different combinations of the datasets.

	CMB	CMB + CMASS	CMB + CMASS + BAO + H_0
α/α_0	$0.9909^{+0.0055}_{-0.0055}$	$0.9910^{+0.0055}_{-0.0055}$	$0.9901^{+0.0055}_{-0.0054}$
$m_e/(m_e)_0$	$1.012^{+0.073}_{-0.073}$	$1.004^{+0.025}_{-0.025}$	$1.028^{+0.019}_{-0.019}$
100Θ	$1.036^{+0.051}_{-0.052}$	$1.031^{+0.015}_{-0.015}$	$1.0467^{+0.0095}_{-0.0094}$
$100\omega_{\rm b}$	$2.24^{+0.18}_{-0.18}$	$2.216^{+0.059}_{-0.059}$	$2.265^{+0.046}_{-0.046}$
$100\omega_{\rm dm}$	$11.29^{+0.92}_{-0.92}$	$11.20^{+0.65}_{-0.66}$	$11.83^{+0.56}_{-0.55}$
τ	$0.0879^{+0.0066}_{-0.0074}$	$0.0877^{+0.0067}_{-0.0071}$	$0.0848^{+0.0063}_{-0.0071}$
$n_{\rm s}$	$0.978^{+0.014}_{-0.014}$	$0.978^{+0.013}_{-0.013}$	$0.977^{+0.012}_{-0.012}$
$\ln(10^{10}A_{\rm s})$	$3.105^{+0.035}_{-0.035}$	$3.104^{+0.035}_{-0.035}$	$3.114^{+0.033}_{-0.033}$
$\Omega_{\rm DE}$	$0.69^{+0.11}_{-0.12}$	$0.706^{+0.020}_{-0.020}$	$0.719^{+0.010}_{-0.010}$
$\Omega_{\rm m}$	$0.31^{+0.12}_{-0.11}$	$0.294^{+0.020}_{-0.020}$	$0.281^{+0.010}_{-0.010}$
σ_8	$0.824^{+0.078}_{-0.081}$	$0.820^{+0.042}_{-0.043}$	$0.860^{+0.036}_{-0.035}$
t_0/Gyr	$14.0^{+1.7}_{-1.7}$	$14.04^{+0.47}_{-0.47}$	$13.56^{+0.27}_{-0.28}$
$z_{\rm re}$	$10.9^{+1.5}_{-1.5}$	$10.8^{+1.3}_{-1.3}$	$11.0^{+1.3}_{-1.3}$
h	$0.70^{+0.16}_{-0.16}$	$0.677^{+0.033}_{-0.033}$	$0.708^{+0.017}_{-0.017}$

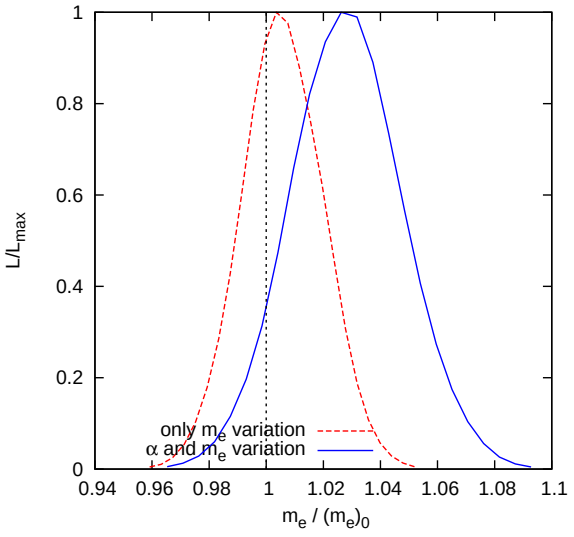

Figure 8. The marginalized, one-dimensional likelihood distribution for the electron mass, when only m_e is allowed to vary, and in the case of the joint variation of α and m_e.

3.4 Variation of fundamental constants and $w_{\rm DE}$

Until now, we have assumed that the dark energy component corresponds to a cosmological constant, with a fixed equation of state specified by $w_{\rm DE} = -1$. In this Section we explore the constraints on the value of $w_{\rm DE}$, assumed to be redshift-independent, in the context of the variation of fundamental constants.

In this study, the dynamical dark energy models are allowed to cross the so-called phantom divide, $w_{\rm DE} = -1$, to explore models with $w_{\rm DE} < -1$. In the framework of general relativity, a single scalar field cannot cross this threshold, since it becomes gravitationally unstable (Feng et al. 2005; Vikman 2005; Hu 2005; Xia et al. 2008). Thus, more degrees of freedom are required, which are difficult to implement in general dark energy studies. We follow the parametrized post-Friedmann (PPF) approach of Fang et al. (2008), as implemented in CAMB, which provides a simple solution to these problems for models in which the dark energy component is smooth compared to the dark matter.

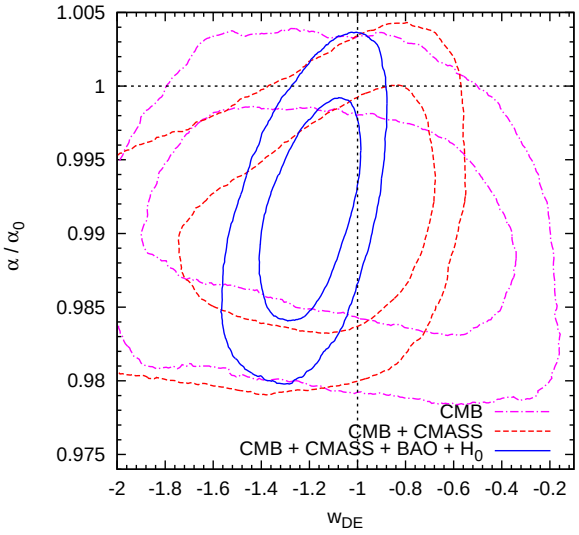

Figure 9. The marginalized posterior distribution in the α - $w_{\rm DE}$ plane for the ΛCDM parameter set extended to include the variation of α and the redshift-independent value of $w_{\rm DE}$ as an additional parameter. The dot-dashed lines show the 68% and 95% contours obtained using CMB information alone. The dashed lines correspond to the results obtained from the combination of CMB data plus the shape of the CMASS $\xi(s)$. The solid lines indicate the results obtained from the full dataset combination (CMB+CMASS+BAO+H_0). The vertical and horizontal dotted lines correspond to the ΛCDM model, with $\alpha/\alpha_0 = 1$ and $w_{\rm DE} = -1$.

First, we perform a statistical analysis varying α and $w_{\rm DE}$, together with the rest of the cosmological parameters. Fig. 9 presents the constraints on the α - $w_{\rm DE}$ plane. Again, the inclusion of additional datasets reduces the allowed region in the parameter space, while increasing the anti-correlation between the fundamental constants. The correlation factor is −0.16, 0.37, and 0.54 for CMB, CMB+CMASS, and the full dataset combination (CMB+CMASS+BAO+H_0), respectively. For the full dataset, the value $w_{\rm DE} \geqslant -1$ is excluded at more than 1 σ.

Table 4 shows the constraints obtained for α, $w_{\rm DE}$, and the cosmological parameters. The inclusion of more datasets slightly improves the constraint on α and does not appreciably affect the mean value. In the case of $w_{\rm DE}$, a large improvement is observed, and the mean value of $w_{\rm DE}$ shifts towards lower values. Our final bounds, using the complete dataset, are $\alpha/\alpha_0 = 0.9915 \pm 0.0048$ and $w_{\rm DE} = -1.20 \pm 0.13$. Our results are consistent with no variation of α at the 2 σ level, while $w_{\rm DE}$ is compatible with a cosmological constant

Table 4. The marginalized 68% allowed regions on the cosmological parameters of the ΛCDM model, adding the variation of the fine structure constant α, and the dark energy equation of state $w_{\rm DE}$, obtained using different combinations of the datasets.

	CMB	CMB + CMASS	CMB + CMASS + BAO + H_0
$w_{\rm DE}$	$-1.07^{+0.48}_{-0.50}$	$-1.23^{+0.36}_{-0.41}$	$-1.20^{+0.13}_{-0.13}$
α/α_0	$0.9908^{+0.0054}_{-0.0054}$	$0.9907^{+0.0049}_{-0.0050}$	$0.9915^{+0.0048}_{-0.0048}$
100Θ	$1.0280^{+0.0077}_{-0.0078}$	$1.0277^{+0.0070}_{-0.0071}$	$1.0289^{+0.0068}_{-0.0068}$
$100\omega_{\rm b}$	$2.205^{+0.042}_{-0.042}$	$2.202^{+0.042}_{-0.042}$	$2.200^{+0.039}_{-0.040}$
$100\omega_{\rm dm}$	$11.18^{+0.48}_{-0.48}$	$11.22^{+0.46}_{-0.47}$	$11.42^{+0.35}_{-0.35}$
τ	$0.0883^{+0.0063}_{-0.0075}$	$0.0866^{+0.0063}_{-0.0073}$	$0.0857^{+0.0064}_{-0.0069}$
$n_{\rm s}$	$0.978^{+0.014}_{-0.014}$	$0.976^{+0.013}_{-0.013}$	$0.973^{+0.013}_{-0.012}$
$\ln(10^{10}A_{\rm s})$	$3.107^{+0.034}_{-0.034}$	$3.104^{+0.033}_{-0.032}$	$3.107^{+0.031}_{-0.031}$
$\Omega_{\rm DE}$	$0.69^{+0.13}_{-0.14}$	$0.736^{+0.063}_{-0.057}$	$0.733^{+0.014}_{-0.014}$
$\Omega_{\rm m}$	$0.31^{+0.14}_{-0.13}$	$0.264^{+0.057}_{-0.063}$	$0.267^{+0.014}_{-0.014}$
σ_8	$0.83^{+0.15}_{-0.14}$	$0.88^{+0.12}_{-0.11}$	$0.882^{+0.045}_{-0.045}$
t_0/Gyr	$14.19^{+0.44}_{-0.43}$	$14.08^{+0.20}_{-0.20}$	$14.04^{+0.18}_{-0.18}$
$z_{\rm re}$	$10.9^{+1.3}_{-1.3}$	$10.7^{+1.3}_{-1.2}$	$10.7^{+1.2}_{-1.2}$
h	$0.70^{+0.16}_{-0.15}$	$0.728^{+0.098}_{-0.087}$	$0.715^{+0.021}_{-0.021}$

also within 2 σ, although at 1 σ, both quantities differ from their standard values.

There is a slight tension at the 1 σ level in the values of some of the cosmological parameters with respect to their values in the ΛCDM model. At 2 σ, however, the results are consistent. Indeed, when compared to the ΛCDM model, we find that the value of Θ is lower and the age of the universe is higher for all of the datasets. The value of n_s is higher for the CMB and the CMB+CMASS datasets, and σ_8 is higher for the full dataset.

We then perform a statistical analysis varying m_e and $w_{\rm DE}$. Fig. 10 presents the resulting constraints on the m_e - $w_{\rm DE}$ plane. CMB data alone cannot place strong constraints on the value of m_e and $w_{\rm DE}$. The inclusion of the CMASS correlation function restricts the allowed region in the parameter space, reducing the allowed range of values of m_e by a factor of two. Using the full dataset, our bounds are $m_e/(m_e)_0 = 0.996 \pm 0.029$ and $w_{\rm DE} = -1.12 \pm 0.23$. In Table 5 we also present the constraints on the other cosmological parameters. The standard case of $m_e = (m_e)_0$ and $w_{\rm DE} = -1$ is completely consistent with all of the datasets. The values of the cosmological parameters are consistent within 1 σ with their values in the ΛCDM model.

3.5 Variation of fundamental constants and f_ν

In the standard ΛCDM scenario, the dark matter component is given entirely by cold dark matter. However, neutrino oscillations found in recent experiments imply that they have a non-zero mass that contributes to the total energy budget of the universe. A variation in the neutrino mass can alter the redshift of matter-radiation equality, thus modifying the CMB power spectrum. Furthermore, until they

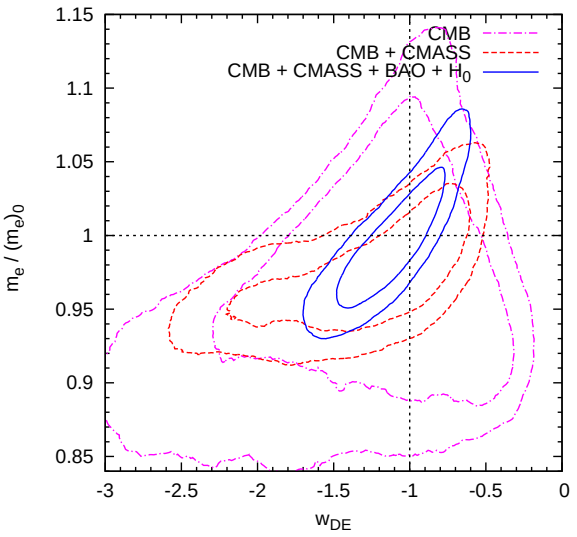

Figure 10. The marginalized posterior distribution in the m_e - $w_{\rm DE}$ plane for the ΛCDM parameter set extended to include the variation of m_e and the redshift-independent value of $w_{\rm DE}$ as an additional parameter. The dot-dashed lines show the 68% and 95% contours obtained using CMB information alone. The dashed lines correspond to the results obtained from the combination of CMB data plus the shape of the CMASS $\xi(s)$. The solid lines indicate the results obtained from the full dataset combination (CMB+CMASS+BAO+H_0). The vertical and horizontal dotted lines correspond to the ΛCDM model, with $m_e/(m_e)_0 = 1$ and $w_{\rm DE} = -1$.

Table 5. The marginalized 68% allowed regions on the cosmological parameters of the ΛCDM model, adding the variation of the electron mass m_e, and the dark energy equation of state $w_{\rm DE}$, obtained using different combinations of the datasets.

	CMB	CMB + CMASS	CMB + CMASS + BAO + H_0
$w_{\rm DE}$	$-1.31^{+0.59}_{-0.64}$	$-1.30^{+0.48}_{-0.56}$	$-1.12^{+0.23}_{-0.23}$
$m_e/(m_e)_0$	$0.962^{+0.060}_{-0.061}$	$0.974^{+0.029}_{-0.029}$	$0.996^{+0.029}_{-0.029}$
100Θ	$1.012^{+0.045}_{-0.045}$	$1.022^{+0.022}_{-0.021}$	$1.037^{+0.021}_{-0.021}$
$100\omega_{\rm b}$	$2.13^{+0.15}_{-0.15}$	$2.156^{+0.078}_{-0.076}$	$2.204^{+0.076}_{-0.075}$
$100\Omega_{\rm dm}$	$10.78^{+0.82}_{-0.81}$	$10.90^{+0.64}_{-0.64}$	$11.52^{+0.62}_{-0.62}$
τ	$0.0845^{+0.0065}_{-0.0073}$	$0.0849^{+0.0067}_{-0.0070}$	$0.0816^{+0.0060}_{-0.0068}$
$n_{\rm s}$	$0.963^{+0.012}_{-0.012}$	$0.963^{+0.011}_{-0.010}$	$0.9613^{+0.0099}_{-0.0100}$
$\ln(10^{10}A_{\rm s})$	$3.077^{+0.031}_{-0.031}$	$3.078^{+0.030}_{-0.031}$	$3.087^{+0.029}_{-0.029}$
$\Omega_{\rm DE}$	$0.69^{+0.15}_{-0.17}$	$0.743^{+0.073}_{-0.063}$	$0.729^{+0.019}_{-0.019}$
$\Omega_{\rm m}$	$0.31^{+0.17}_{-0.15}$	$0.257^{+0.063}_{-0.073}$	$0.271^{+0.019}_{-0.019}$
σ_8	$0.83^{+0.15}_{-0.15}$	$0.85^{+0.12}_{-0.11}$	$0.852^{+0.049}_{-0.048}$
t_0/Gyr	$14.8^{+1.6}_{-1.6}$	$14.30^{+0.56}_{-0.56}$	$13.86^{+0.55}_{-0.56}$
$z_{\rm re}$	$9.9^{+1.3}_{-1.3}$	$10.1^{+1.2}_{-1.2}$	$10.2^{+1.2}_{-1.2}$
h	$0.70^{+0.20}_{-0.19}$	$0.730^{+0.11}_{-0.091}$	$0.712^{+0.021}_{-0.020}$

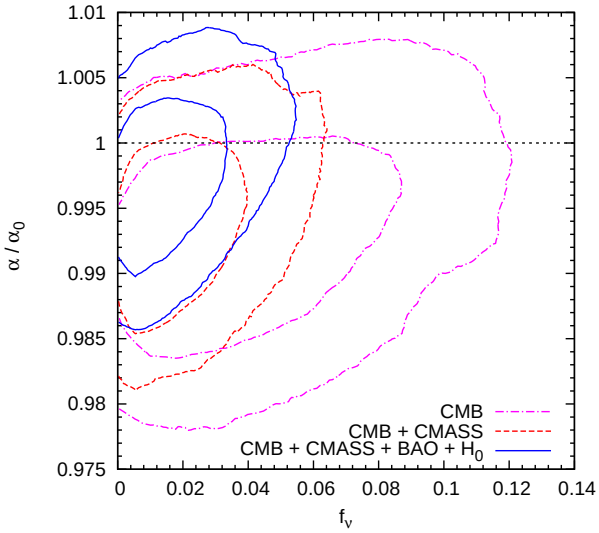

Figure 11. The marginalized posterior distribution in the α - f_ν plane for the ΛCDM parameter set extended to include the variation of α and a non-negligible fraction of massive neutrinos. The dot-dashed lines show the 68% and 95% contours obtained using CMB information alone. The dashed lines correspond to the results obtained from the combination of CMB data plus the shape of the CMASS $\xi(s)$. The solid lines indicate the results obtained from the full dataset combination (CMB+CMASS+BAO+H_0).

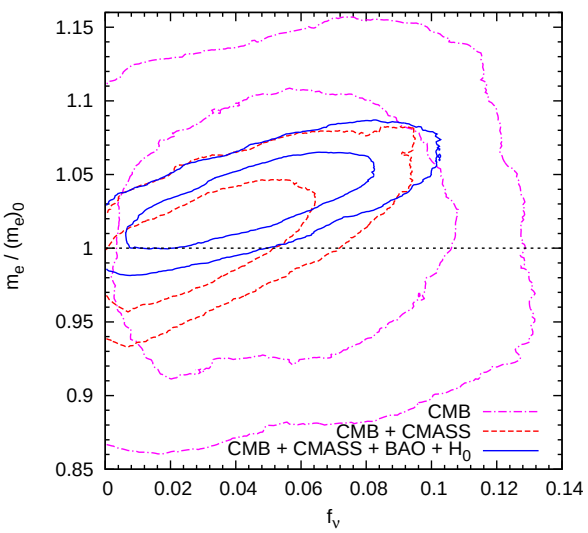

Figure 12. The marginalized posterior distribution in the m_e - f_ν plane for the ΛCDM parameter set extended to include the variation of m_e and a non-negligible fraction of massive neutrinos. The dot-dashed lines show the 68% and 95% contours obtained using CMB information alone. The dashed lines correspond to the results obtained from the combination of CMB data plus the shape of the CMASS $\xi(s)$. The solid lines indicate the results obtained from the full dataset combination (CMB+CMASS+BAO+H_0).

become non-relativistic, neutrinos free-stream out of density perturbations, suppressing the growth of structures on scales smaller than the horizon at that time, which depends on their mass, thus affecting the shape of the matter power spectrum and the correlation function. In this Section we explore the constraints on the neutrino fraction, f_ν, when one of the fundamental constants (α or m_e) is allowed to vary. We assume three neutrino species of equal mass.

Fig. 11 shows the contours in the α - f_ν plane. The constraints on α are only slightly poorer than in the $f_\nu = 0$ case. When additional datasets are incorporated to the fit, the bounds on α tighten.

In Table 6 we present the constraints obtained for α, f_ν, and the remaining cosmological parameters. In the case of only CMB data, we find $f_\nu < 0.098$ at 95% CL, and $\alpha/\alpha_0 = 0.9933^{+0.0057}_{-0.0058}$. When we also include the information from the CMASS correlation function, this limit is reduced to $f_\nu < 0.049$ at 95% CL, and the constraint on α is $\alpha/\alpha_0 = 0.9940^{+0.0050}_{-0.0049}$. The constraints for the full data set are $f_\nu < 0.043$ at 95% CL and $\alpha/\alpha_0 = 0.9978^{+0.0044}_{-0.0045}$. We find no degeneracy between α and f_ν. When all datasets are included in the analysis, the value of α is increased (due to the larger value of h), our results being consistent with no variation of α within 1 σ.

Regarding the constraints on the primary cosmological parameters, we find that they are consistent with the ΛCDM values at 1 σ in most of the cases. For the CMB and CMB+CMASS datasets, some of the derived parameters differ by more than 1 σ from their values in the ΛCDM model, but they are consistent within 1 σ when we consider the full dataset, with exception of σ_8, which is lower by more than 1 σ also for the full dataset. For the CMB dataset, h differs by more than 2 σ from the ΛCDM value, by 1 σ for the CMB+CMASS dataset, and is fully consistent for the full dataset. The constraints at 95% CL on the sum of the neutrinos masses are $\sum m_\nu < 1.2\,\mathrm{eV}$ (CMB), $\sum m_\nu < 0.53\,\mathrm{eV}$ (CMB+CMASS), and $\sum m_\nu < 0.46\,\mathrm{eV}$ (full dataset).

Fig. 12 shows the contours for the analysis in the m_e - f_ν plane. The precision in the constraints on m_e are similar as those in the $f_\nu = 0$ case. When the CMASS correlation function is added to the CMB dataset, the allowed region in the parameter space is reduced. Due to the degeneracy between H_0 and m_e, and between the latter and f_ν (correlation factor equal to 0.83 and 0.72, respectively), when the full dataset is considered, the contours are shifted towards a region with higher values of m_e and f_ν.

In Table 7 we present the constraints obtained for m_e, f_ν, and the cosmological parameters. In the case of only CMB data, we find $f_\nu < 0.11$ at 95% CL, and $m_e/(m_e)_0 = 1.011^{+0.067}_{-0.066}$. When we also include the information from the CMASS correlation function, this limit is reduced to $f_\nu < 0.074$ at 95% CL, and the constraint on m_e is $m_e/(m_e)_0 = 1.009^{+0.029}_{-0.028}$. The constraints for the full data set are $f_\nu < 0.086$ at 95% CL and $m_e/(m_e)_0 = 1.035 \pm 0.021$. When all datasets are included in the analysis, the value of m_e is increased (due to the larger value of h), and our results are consistent with no variation of m_e at 2 σ.

With regards to the constraints on the cosmological parameters, we find that they are consistent with the ΛCDM values at 1 σ in most of the cases, although $\omega_{\rm dm}$ differs from the ΛCDM value by 1 σ for the full dataset. There is also tension for σ_8 at the 1 σ level for all of the datasets, in the sense that our constraints are lower than the ΛCDM values. For the full dataset, the age of the universe is lower and h is higher by more than 1 σ than their corresponding

Table 6. The marginalized 68% allowed regions on the cosmological parameters of the ΛCDM model, adding the variation of the fine structure constant α and f_ν as a free parameter, obtained using different combinations of the datasets.

	CMB	CMB + CMASS	CMB + CMASS + BAO + H_0
f_ν	< 0.098 (95% CL)	< 0.049 (95% CL)	< 0.043 (95% CL)
α/α_0	$0.9933^{+0.0057}_{-0.0058}$	$0.9940^{+0.0050}_{-0.0049}$	$0.9978^{+0.0044}_{-0.0045}$
100Θ	$1.0312^{+0.0081}_{-0.0082}$	$1.0326^{+0.0071}_{-0.0069}$	$1.0382^{+0.0061}_{-0.0062}$
$100\omega_{\rm b}$	$2.187^{+0.044}_{-0.044}$	$2.209^{+0.039}_{-0.038}$	$2.228^{+0.038}_{-0.037}$
$100\omega_{\rm dm}$	$11.86^{+0.71}_{-0.70}$	$11.25^{+0.39}_{-0.39}$	$11.27^{+0.34}_{-0.34}$
τ	$0.0857^{+0.0061}_{-0.0072}$	$0.0889^{+0.0068}_{-0.0075}$	$0.0869^{+0.0063}_{-0.0070}$
$n_{\rm s}$	$0.968^{+0.016}_{-0.016}$	$0.974^{+0.013}_{-0.013}$	$0.972^{+0.013}_{-0.012}$
$\ln(10^{10}A_{\rm s})$	$3.097^{+0.034}_{-0.034}$	$3.094^{+0.033}_{-0.032}$	$3.086^{+0.031}_{-0.031}$
$\sum m_\nu$	$< 1.2\,$eV (95% CL)	$< 0.53\,$eV (95% CL)	$< 0.46\,$eV (95% CL)
$\Omega_{\rm DE}$	$0.636^{+0.062}_{-0.062}$	$0.696^{+0.020}_{-0.020}$	$0.714^{+0.011}_{-0.011}$
$\Omega_{\rm m}$	$0.364^{+0.062}_{-0.062}$	$0.304^{+0.020}_{-0.020}$	$0.286^{+0.011}_{-0.011}$
σ_8	$0.715^{+0.073}_{-0.074}$	$0.761^{+0.043}_{-0.044}$	$0.772^{+0.038}_{-0.039}$
t_0/Gyr	$14.32^{+0.28}_{-0.28}$	$14.11^{+0.20}_{-0.20}$	$13.90^{+0.16}_{-0.16}$
$z_{\rm re}$	$10.8^{+1.3}_{-1.2}$	$10.9^{+1.3}_{-1.3}$	$10.6^{+1.2}_{-1.2}$
h	$0.626^{+0.041}_{-0.041}$	$0.666^{+0.019}_{-0.019}$	$0.688^{+0.012}_{-0.012}$

Table 7. The marginalized 68% allowed regions on the cosmological parameters of the ΛCDM model, adding the variation of the electron mass m_e and f_ν as a free parameter, obtained using different combinations of the datasets.

	CMB	CMB + CMASS	CMB + CMASS + BAO + H_0
f_ν	< 0.11(95%CL)	< 0.074(95%CL)	< 0.086(95%CL)
$m_e/(m_e)_0$	$1.011^{+0.067}_{-0.066}$	$1.009^{+0.029}_{-0.028}$	$1.035^{+0.021}_{-0.021}$
100Θ	$1.048^{+0.048}_{-0.047}$	$1.047^{+0.021}_{-0.020}$	$1.065^{+0.014}_{-0.015}$
$100\omega_{\rm b}$	$2.22^{+0.16}_{-0.16}$	$2.225^{+0.065}_{-0.064}$	$2.276^{+0.047}_{-0.048}$
$100\omega_{\rm dm}$	$12.2^{+1.1}_{-1.1}$	$11.81^{+0.92}_{-0.89}$	$12.60^{+0.77}_{-0.76}$
τ	$0.0840^{+0.0063}_{-0.0073}$	$0.0839^{+0.0061}_{-0.0072}$	$0.0818^{+0.0061}_{-0.0067}$
$n_{\rm s}$	$0.957^{+0.013}_{-0.014}$	$0.962^{+0.010}_{-0.010}$	$0.9593^{+0.0098}_{-0.0099}$
$\ln(10^{10}A_{\rm s})$	$3.081^{+0.030}_{-0.031}$	$3.081^{+0.031}_{-0.031}$	$3.089^{+0.029}_{-0.030}$
$\sum m_\nu$	$< 1.4\,$eV (95% CL)	$< 0.91\,$eV (95% CL)	$< 1.1\,$eV (95% CL)
$\Omega_{\rm DE}$	$0.64^{+0.13}_{-0.14}$	$0.702^{+0.021}_{-0.021}$	$0.711^{+0.012}_{-0.011}$
$\Omega_{\rm m}$	$0.36^{+0.14}_{-0.13}$	$0.297^{+0.021}_{-0.021}$	$0.289^{+0.011}_{-0.012}$
σ_8	$0.694^{+0.090}_{-0.091}$	$0.745^{+0.048}_{-0.050}$	$0.748^{+0.054}_{-0.055}$
t_0/Gyr	$14.0^{+1.6}_{-1.5}$	$13.76^{+0.52}_{-0.54}$	$13.28^{+0.33}_{-0.33}$
$z_{\rm re}$	$10.7^{+1.4}_{-1.4}$	$10.6^{+1.3}_{-1.3}$	$10.8^{+1.3}_{-1.3}$
h	$0.67^{+0.15}_{-0.15}$	$0.689^{+0.037}_{-0.035}$	$0.718^{+0.019}_{-0.019}$

values in the ΛCDM model. The constraints at 95% CL on the sum of the neutrinos masses are $\sum m_\nu < 1.4\,$eV (CMB), $\sum m_\nu < 0.91\,$eV (CMB+CMASS), and $\sum m_\nu < 1.1\,$eV (full dataset).

3.6 Variation of fundamental constants and $N_{\rm eff}$

The effective number of relativistic species, $N_{\rm eff}$, has been reported as higher than the expected standard value of $N_{\rm eff} = 3.046$ (Dunkley et al. 2011; Keisler et al. 2011). This may indicate either additional relativistic species, or evidence for non-standard decoupling. Here we study the con-

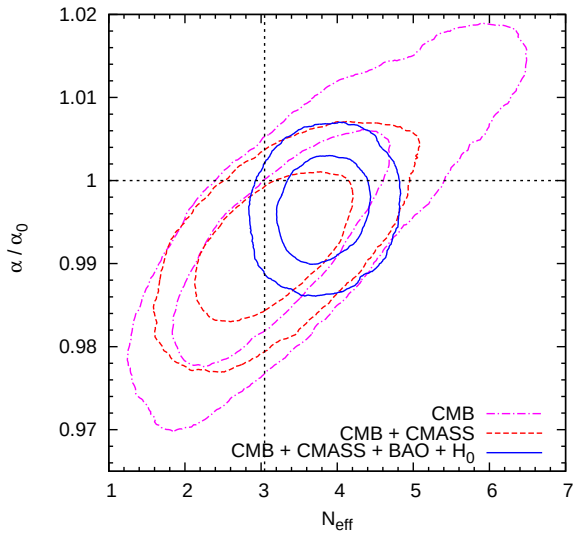

Figure 13. The marginalized posterior distribution in the α - $N_{\rm eff}$ plane for the ΛCDM parameter set extended to include the variation of α and a variable effective number of relativistic degrees of freedom $N_{\rm eff}$. The dot-dashed lines show the 68% and 95% contours obtained using CMB information alone. The dashed lines correspond to the results obtained from the combination of CMB data plus the shape of the CMASS $\xi(s)$. The solid lines indicate the results obtained from the full dataset combination (CMB+CMASS+BAO+H_0).

straints from the CMASS correlation function on the variation of α and m_e when $N_{\rm eff}$ can differ from its standard value, providing details on the constraints set by the different datasets considered in this paper.

In the case of no variation of the fundamental constants, Keisler et al. (2011) present a bound of $N_{\rm eff} = 3.85 \pm 0.62$ for the CMB dataset (WMAP+SPT). We consider the ΛCDM+$N_{\rm eff}$ model and obtain the constraints $N_{\rm eff} = 3.75 \pm 0.58$ for CMB+CMASS and $N_{\rm eff} = 3.86^{+0.39}_{-0.40}$ for the full dataset.

The contours in Fig. 13 show the two-dimensional marginalized constraints in the $N_{\rm eff}$ - α plane. There is a strong degeneracy between α and $N_{\rm eff}$ in the CMB dataset. When we add the CMASS dataset, this degeneracy is partially alleviated, and it disappears for the full dataset. The inclusion of the HST H_0 prior shifts the contours towards higher values of $N_{\rm eff}$ and α, making the latter consistent with its present value at 1 σ.

In Table 8 we present the constraints on $N_{\rm eff}$, α, and the rest of the cosmological parameters for all of our datasets. When α is allowed to vary, $N_{\rm eff} = 3.37^{+0.95}_{-0.97}$ for the CMB dataset, which is a value more consistent with the standard one than when α is fixed to its present value (as said before, for WMAP+SPT data, the value presented by Keisler et al. 2011, is $N_{\rm eff} = 3.85 \pm 0.62$). The constraint on α is $\alpha/\alpha_0 = 0.9935 \pm 0.0093$. By adding the CMASS correlation function, we tighten the bounds on $N_{\rm eff}$ and α, which become $N_{\rm eff} = 3.21^{+0.66}_{-0.67}$ and $\alpha/\alpha_0 = 0.9926 \pm 0.0058$. For CMB+CMASS+BAO, $N_{\rm eff} = 3.19 \pm 0.64$ and $\alpha/\alpha_0 = 0.9926^{+0.0054}_{-0.0055}$. When all datasets are considered in the analysis, the constraints are $N_{\rm eff} = 3.83 \pm 0.40$ and $\alpha/\alpha_0 = 0.9967 \pm 0.0042$. The H_0 prior shifts $N_{\rm eff}$ towards higher values, which lie almost 2 σ from the standard value of 3.046. On the other hand, α is consistent with no variation at 1 σ. Menegoni et al. (2012) studied the variation of α when $N_{\rm eff}$ can have values different from the standard one, allowing also for variations in the primordial helium abundance, $Y_{\rm He}$. Their constraints are $\alpha/\alpha_0 = 0.990 \pm 0.006$ and $N_{\rm eff} = 4.10^{+0.24}_{-0.29}$. The difference in the datasets is that they use the DR7 LRG power spectrum and add the ACT data to their analysis, presenting their results only for the full dataset.

Table 8. The marginalized 68% allowed regions on the cosmological parameters of the ΛCDM model, adding the variation of the fine structure constant α and $N_{\rm eff}$ as a free parameter, obtained using different combinations of the datasets.

	CMB	CMB + CMASS	CMB + CMASS + BAO + H_0
$N_{\rm eff}$	$3.37^{+0.95}_{-0.97}$	$3.21^{+0.66}_{-0.67}$	$3.83^{+0.40}_{-0.40}$
α/α_0	$0.9935^{+0.0093}_{-0.0093}$	$0.9926^{+0.0058}_{-0.0058}$	$0.9967^{+0.0042}_{-0.0042}$
100Θ	$1.032^{+0.012}_{-0.012}$	$1.0304^{+0.0075}_{-0.0074}$	$1.0349^{+0.0057}_{-0.0058}$
$100\omega_{\rm b}$	$2.228^{+0.079}_{-0.079}$	$2.218^{+0.055}_{-0.055}$	$2.254^{+0.041}_{-0.041}$
$100\omega_{\rm dm}$	$11.7^{+1.7}_{-1.8}$	$11.4^{+1.3}_{-1.4}$	$12.72^{+0.88}_{-0.87}$
τ	$0.0886^{+0.0063}_{-0.0074}$	$0.0882^{+0.0064}_{-0.0073}$	$0.0878^{+0.0065}_{-0.0072}$
$n_{\rm s}$	$0.981^{+0.021}_{-0.021}$	$0.979^{+0.017}_{-0.017}$	$0.988^{+0.015}_{-0.015}$
$\ln(10^{10}A_{\rm s})$	$3.112^{+0.049}_{-0.049}$	$3.106^{+0.044}_{-0.045}$	$3.134^{+0.036}_{-0.036}$
$\Omega_{\rm DE}$	$0.705^{+0.050}_{-0.049}$	$0.707^{+0.019}_{-0.019}$	$0.715^{+0.010}_{-0.010}$
$\Omega_{\rm m}$	$0.295^{+0.049}_{-0.050}$	$0.293^{+0.019}_{-0.019}$	$0.285^{+0.010}_{-0.010}$
σ_8	$0.832^{+0.060}_{-0.061}$	$0.822^{+0.048}_{-0.049}$	$0.867^{+0.032}_{-0.032}$
t_0/Gyr	$13.8^{+1.3}_{-1.3}$	$13.95^{+0.81}_{-0.79}$	$13.20^{+0.38}_{-0.38}$
$z_{\rm re}$	$10.9^{+1.3}_{-1.3}$	$10.9^{+1.3}_{-1.3}$	$11.1^{+1.3}_{-1.3}$
h	$0.696^{+0.092}_{-0.092}$	$0.683^{+0.047}_{-0.048}$	$0.725^{+0.022}_{-0.022}$

There is tension at the 1 σ level in some of the cosmological parameters with respect to their ΛCDM model values. For the full dataset, Θ and t_0 are more than 1 σ lower, and $n_{\rm s}$, σ_8, h and $\omega_{\rm dm}$ are larger by more than 1 σ. Θ is also more than 1 σ lower than its concordance value for the CMB+CMASS dataset. In the rest of the cases, the parameters are all consistent within 1 σ with their ΛCDM values.

We now analyze the results for the case in which m_e and $N_{\rm eff}$ are allowed to vary. In Fig. 14 we show the two-dimensional marginalized constraints in the $N_{\rm eff}$ - m_e plane. There is no degeneracy between m_e and $N_{\rm eff}$ for the CMB and CMB+CMASS datasets. When the full dataset is considered, a mild correlation between both quantities appears.

In Table 9 we present the constraints on $N_{\rm eff}$, m_e, and the rest of the cosmological parameters for all of our datasets. For the CMB dataset, $N_{\rm eff} = 3.86 \pm 0.60$, which is more than 1 σ higher than the standard value. The constraint on m_e is $m_e/(m_e)_0 = 0.988 \pm 0.065$. By adding the CMASS correlation function, we significantly tighten the bounds on m_e but only slightly improve the limits on $N_{\rm eff}$, which become $N_{\rm eff} = 3.80 \pm 0.57$ and $m_e/(m_e)_0 = 0.981 \pm 0.020$. For CMB+CMASS+BAO, $N_{\rm eff} = 3.78 \pm 0.58$ and $m_e/(m_e)_0 = 0.981 \pm 0.018$. When all datasets are con-

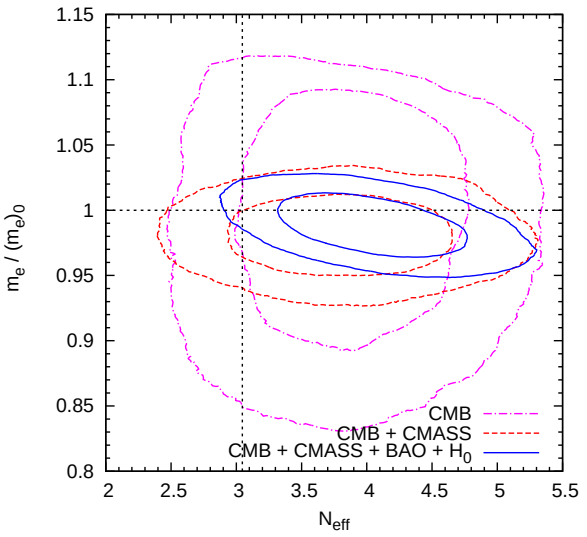

Figure 14. The marginalized posterior distribution in the m_e - $N_{\rm eff}$ plane for the ΛCDM parameter set extended to include the variation of m_e and a variable effective number of relativistic degrees of freedom $N_{\rm eff}$. The dot-dashed lines show the 68% and 95% contours obtained using CMB information alone. The dashed lines correspond to the results obtained from the combination of CMB data plus the shape of the CMASS $\xi(s)$. The solid lines indicate the results obtained from the full dataset combination (CMB+CMASS+BAO+H_0).

Table 9. The marginalized 68% allowed regions on the cosmological parameters of the ΛCDM model, adding the variation of the electron mass m_e and $N_{\rm eff}$ as a free parameter, obtained using different combinations of the datasets.

	CMB	CMB + CMASS	CMB + CMASS + BAO + H_0
$N_{\rm eff}$	$3.86^{+0.60}_{-0.60}$	$3.80^{+0.57}_{-0.57}$	$4.04^{+0.47}_{-0.46}$
$m_e/(m_e)_0$	$0.988^{+0.065}_{-0.065}$	$0.981^{+0.020}_{-0.020}$	$0.988^{+0.015}_{-0.016}$
100Θ	$1.030^{+0.048}_{-0.048}$	$1.026^{+0.015}_{-0.015}$	$1.031^{+0.011}_{-0.011}$
$100\omega_{\rm b}$	$2.24^{+0.17}_{-0.17}$	$2.216^{+0.062}_{-0.062}$	$2.245^{+0.042}_{-0.042}$
$100\omega_{\rm dm}$	$12.4^{+1.5}_{-1.4}$	$12.2^{+1.2}_{-1.2}$	$12.85^{+0.82}_{-0.80}$
τ	$0.0891^{+0.0067}_{-0.0075}$	$0.0884^{+0.0065}_{-0.0075}$	$0.0882^{+0.0066}_{-0.0075}$
$n_{\rm s}$	$0.986^{+0.019}_{-0.020}$	$0.985^{+0.017}_{-0.017}$	$0.990^{+0.016}_{-0.016}$
$\ln(10^{10}A_{\rm s})$	$3.124^{+0.044}_{-0.045}$	$3.119^{+0.042}_{-0.042}$	$3.134^{+0.036}_{-0.036}$
$\Omega_{\rm DE}$	$0.69^{+0.11}_{-0.11}$	$0.709^{+0.020}_{-0.020}$	$0.715^{+0.011}_{-0.011}$
$\Omega_{\rm m}$	$0.31^{+0.11}_{-0.11}$	$0.291^{+0.020}_{-0.020}$	$0.285^{+0.011}_{-0.011}$
σ_8	$0.844^{+0.085}_{-0.086}$	$0.835^{+0.049}_{-0.049}$	$0.862^{+0.033}_{-0.033}$
t_0/Gyr	$13.4^{+1.6}_{-1.6}$	$13.53^{+0.65}_{-0.65}$	$13.14^{+0.34}_{-0.34}$
$z_{\rm re}$	$10.9^{+1.5}_{-1.5}$	$10.7^{+1.3}_{-1.3}$	$10.9^{+1.3}_{-1.3}$
h	$0.73^{+0.16}_{-0.16}$	$0.705^{+0.042}_{-0.043}$	$0.728^{+0.020}_{-0.020}$

sidered in the analysis, the constraints are $N_{\rm eff} = 4.04^{+0.47}_{-0.46}$ and $m_e/(m_e)_0 = 0.988^{+0.015}_{-0.016}$. The H_0 prior shifts $N_{\rm eff}$ towards even higher values, which are more than 2 σ above the standard value of 3.046. On the other hand, m_e is consistent with no variation at the 1 σ level for all of the datasets.

Regarding the values of the remaining cosmological parameters, they are all consistent within 1 σ with their ΛCDM values for the CMB dataset. For the CMB+CMASS dataset, $n_{\rm s}$ is higher than its standard value by more than 1 σ. For the full dataset, $\omega_{\rm dm}$, $n_{\rm s}$, σ_8, and h are higher than their standard values in more than 1 σ, while t_0 is lower in more than 1 σ.

3.7 Variation of fundamental constants and $Y_{\rm He}$

Light nuclei begin to form in a process known as big bang nucleosynthesis (BBN, Alpher et al. 1948; Schramm & Turner 1998; Steigman 2007), when the universe cools to $T \sim 0.1$ MeV. We denote the primordial abundance (mass fraction) of ^{4}He as $Y_{\rm He}$, which is a function of the baryon density and the expansion rate during BBN. The value of $Y_{\rm He}$ can be estimated by the effect of helium on the CMB damping tail. Helium combines earlier than hydrogen, and thus more helium (at fixed baryon density) leads to fewer free electrons during hydrogen recombination. This, in turn, leads to larger diffusion lengths for photons and less power in the CMB damping tail. We study the constraints from the CMASS correlation function on the variation of α and m_e when $Y_{\rm He}$ can differ from its standard value of $Y_{\rm He} = 0.24$.

In the case of no variation of the fundamental constants, Keisler et al. (2011) present a bound of $Y_{\rm He} = 0.296 \pm 0.030$ for the CMB dataset (WMAP+SPT). We consider the ΛCDM+$Y_{\rm He}$ model and obtain the constraints $Y_{\rm He} = 0.297 \pm 0.030$ for CMB+CMASS and $Y_{\rm He} = 0.301^{+0.028}_{-0.029}$ for the full dataset.

The contours in Fig. 15 show the two-dimensional marginalized constraints in the $Y_{\rm He}$ - α plane. There is a strong degeneracy between α and $Y_{\rm He}$ in all of the datasets. When α is allowed to vary, CMB information alone is insufficient to place any reliable constraint on $Y_{\rm He}$. When the CMASS dataset is added, the constraint improves noticeably. The inclusion of the HST H_0 prior improves further the constraints, and shifts the contours towards higher values of $Y_{\rm He}$ and α, making the former measurement inconsistent with its standard value at 1 σ.

In Table 10 we present the constraints on $Y_{\rm He}$, α, and the rest of the cosmological parameters for all of our datasets. When α is allowed to vary, $Y_{\rm He} = 0.26 \pm 0.15$ for the CMB dataset, which is a value consistent with the standard one, contrary to the case when α is fixed to its present value (for WMAP+SPT data, the value presented by Keisler et al. 2011, is $Y_{\rm He} = 0.296 \pm 0.030$). The constraint on α is $\alpha/\alpha_0 = 0.994^{+0.026}_{-0.025}$. By adding the CMASS correlation function, we tighten the bounds on $Y_{\rm He}$ and α to $Y_{\rm He} = 0.249 \pm 0.064$ and $\alpha/\alpha_0 = 0.9920^{+0.0092}_{-0.0093}$. When all datasets are considered in the analysis, the constraints are $Y_{\rm He} = 0.314 \pm 0.043$ and $\alpha/\alpha_0 = 1.0023^{+0.0062}_{-0.0061}$. The H_0 prior shifts $Y_{\rm He}$ towards higher values, which are almost 2 σ above the standard value of 0.24. On the other hand, α is consistent with no variation at 1 σ. Menegoni et al. (2012) studied the joint variation of α, $N_{\rm eff}$ and $Y_{\rm He}$; their con-

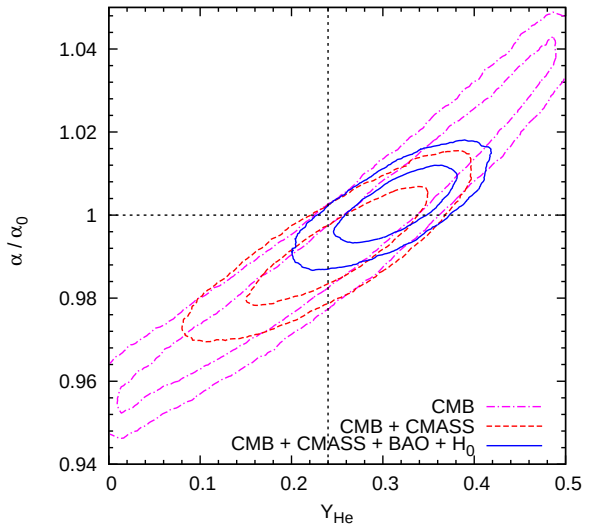

Figure 15. The marginalized posterior distribution in the α - $Y_{\rm He}$ plane for the ΛCDM parameter set extended to include the variation of α and a variable primordial helium abundance $Y_{\rm He}$. The dot-dashed lines show the 68% and 95% contours obtained using CMB information alone. The dashed lines correspond to the results obtained from the combination of CMB data plus the shape of the CMASS $\xi(s)$. The solid lines indicate the results obtained from the full dataset combination (CMB+CMASS+BAO+H_0).

straint is $Y_{\rm He} = 0.215 \pm 0.096$ but with $N_{\rm eff}$ higher by more than 3 σ than its standard value.

There is a slight tension at the 1 σ level for the parameter $n_{\rm s}$, which is higher than its ΛCDM value for the CMB+CMASS and the full datasets. In the rest of the cases, the parameters are all consistent within 1 σ with their ΛCDM values.

We now analyze the results for the case in which m_e and $Y_{\rm He}$ are allowed to vary. Fig. 16 shows the two-dimensional marginalized constraints in the $Y_{\rm He}$ - m_e plane. There is no degeneracy between m_e and $Y_{\rm He}$ for any of the datasets.

In Table 11 we present the constraints on $Y_{\rm He}$, m_e, and the rest of the cosmological parameters for all of our datasets. For the CMB dataset, $Y_{\rm He} = 0.296 \pm 0.029$, which is almost 2 σ higher than the standard value. The constraint on m_e is $m_e/(m_e)_0 = 0.994^{+0.070}_{-0.068}$. By adding the CMASS correlation function, we tighten the bounds on m_e by a factor of three ($m_e/(m_e)_0 = 0.985^{+0.020}_{-0.021}$) but the bound on $Y_{\rm He}$ is unchanged. When all datasets are considered in the analysis, the constraints are $Y_{\rm He} = 0.302 \pm 0.029$ and $m_e/(m_e)_0 = 1.006^{+0.013}_{-0.014}$. The H_0 prior shifts $Y_{\rm He}$ towards slightly higher values, which are more than 2 σ above the standard value of 0.24. On the other hand, m_e is consistent with no variation at 1 σ, for all of the datasets.

Regarding the values of the remaining cosmological parameters, we find that there is a slight tension at the 1 σ level for the parameter $n_{\rm s}$, which is higher than its ΛCDM value for the CMB+CMASS dataset, and for the parameter σ_8, which is higher than its ΛCDM value for the full dataset. In the rest of the cases, the parameters are all consistent within 1 σ with their ΛCDM values.

Table 10. The marginalized 68% allowed regions on the cosmological parameters of the ΛCDM model, adding the variation of the fine structure constant α and $Y_{\rm He}$ as a free parameter, obtained using different combinations of the datasets.

	CMB	CMB + CMASS	CMB + CMASS + BAO + H_0
$Y_{\rm He}$	$0.26^{+0.15}_{-0.15}$	$0.249^{+0.064}_{-0.064}$	$0.314^{+0.043}_{-0.043}$
α/α_0	$0.994^{+0.026}_{-0.025}$	$0.9920^{+0.0092}_{-0.0093}$	$1.0023^{+0.0062}_{-0.0061}$
100Θ	$1.034^{+0.042}_{-0.041}$	$1.030^{+0.015}_{-0.015}$	$1.0466^{+0.0096}_{-0.0096}$
$100\omega_{\rm b}$	$2.23^{+0.15}_{-0.14}$	$2.214^{+0.061}_{-0.060}$	$2.265^{+0.047}_{-0.046}$
$100\omega_{\rm dm}$	$11.26^{+0.78}_{-0.77}$	$11.13^{+0.66}_{-0.66}$	$11.84^{+0.57}_{-0.57}$
τ	$0.0881^{+0.0065}_{-0.0074}$	$0.0878^{+0.0062}_{-0.0073}$	$0.0856^{+0.0063}_{-0.0069}$
$n_{\rm s}$	$0.978^{+0.014}_{-0.015}$	$0.978^{+0.013}_{-0.013}$	$0.977^{+0.013}_{-0.013}$
$\ln(10^{10}A_{\rm s})$	$3.105^{+0.036}_{-0.036}$	$3.102^{+0.036}_{-0.035}$	$3.117^{+0.033}_{-0.033}$
$\Omega_{\rm DE}$	$0.695^{+0.094}_{-0.098}$	$0.705^{+0.020}_{-0.020}$	$0.718^{+0.010}_{-0.010}$
$\Omega_{\rm m}$	$0.305^{+0.098}_{-0.094}$	$0.295^{+0.020}_{-0.020}$	$0.2817^{+0.010}_{-0.010}$
σ_8	$0.822^{+0.068}_{-0.068}$	$0.816^{+0.044}_{-0.044}$	$0.862^{+0.036}_{-0.036}$
t_0/Gyr	$14.0^{+1.4}_{-1.4}$	$14.08^{+0.47}_{-0.47}$	$13.56^{+0.28}_{-0.28}$
$z_{\rm re}$	$10.9^{+1.3}_{-1.3}$	$10.8^{+1.2}_{-1.3}$	$10.9^{+1.3}_{-1.3}$
h	$0.69^{+0.13}_{-0.13}$	$0.674^{+0.032}_{-0.033}$	$0.708^{+0.017}_{-0.017}$

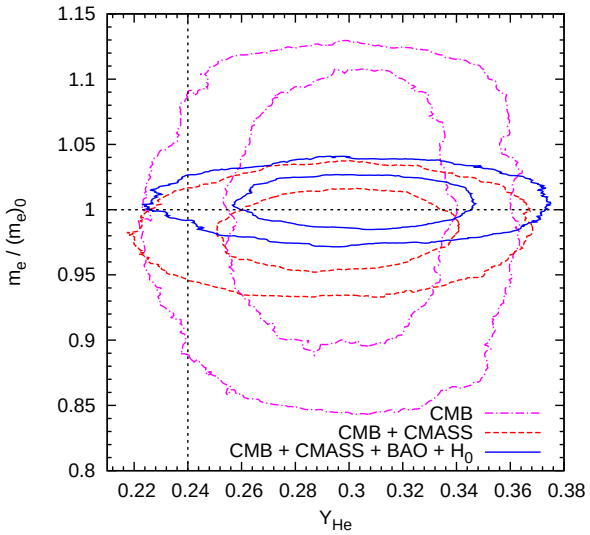

Figure 16. The marginalized posterior distribution in the m_e - $Y_{\rm He}$ plane for the ΛCDM parameter set extended to include the variation of m_e and a variable primordial helium fraction $Y_{\rm He}$. The dot-dashed lines show the 68% and 95% contours obtained using CMB information alone. The dashed lines correspond to the results obtained from the combination of CMB data plus the shape of the CMASS $\xi(s)$. The solid lines indicate the results obtained from the full dataset combination (CMB+CMASS+BAO+H_0).

Table 11. The marginalized 68% allowed regions on the cosmological parameters of the ΛCDM model, adding the variation of the electron mass m_e and $Y_{\rm He}$ as a free parameter, obtained using different combinations of the datasets.

	CMB	CMB + CMASS	CMB + CMASS + BAO + H_0
$Y_{\rm He}$	$0.296^{+0.029}_{-0.029}$	$0.295^{+0.029}_{-0.030}$	$0.302^{+0.029}_{-0.029}$
$m_e/(m_e)_0$	$0.994^{+0.070}_{-0.068}$	$0.985^{+0.020}_{-0.021}$	$1.006^{+0.013}_{-0.014}$
100Θ	$1.037^{+0.051}_{-0.050}$	$1.031^{+0.015}_{-0.015}$	$1.0473^{+0.0094}_{-0.0095}$
$100\omega_{\rm b}$	$2.24^{+0.17}_{-0.17}$	$2.216^{+0.058}_{-0.059}$	$2.267^{+0.046}_{-0.046}$
$100\omega_{\rm dm}$	$11.33^{+0.91}_{-0.92}$	$11.20^{+0.65}_{-0.66}$	$11.87^{+0.55}_{-0.56}$
τ	$0.0881^{+0.0064}_{-0.0075}$	$0.0882^{+0.0065}_{-0.0075}$	$0.0849^{+0.0063}_{-0.0070}$
n_s	$0.978^{+0.014}_{-0.014}$	$0.978^{+0.013}_{-0.013}$	$0.977^{+0.013}_{-0.013}$
$\ln(10^{10}A_{\rm s})$	$3.106^{+0.035}_{-0.035}$	$3.105^{+0.034}_{-0.034}$	$3.116^{+0.033}_{-0.033}$
$\Omega_{\rm DE}$	$0.69^{+0.11}_{-0.11}$	$0.706^{+0.020}_{-0.020}$	$0.718^{+0.010}_{-0.010}$
$\Omega_{\rm m}$	$0.31^{+0.11}_{-0.11}$	$0.294^{+0.020}_{-0.020}$	$0.282^{+0.010}_{-0.010}$
σ_8	$0.827^{+0.077}_{-0.079}$	$0.821^{+0.041}_{-0.042}$	$0.863^{+0.035}_{-0.035}$
t_0/Gyr	$13.9^{+1.6}_{-1.6}$	$14.04^{+0.47}_{-0.47}$	$13.54^{+0.28}_{-0.28}$
$z_{\rm re}$	$10.9^{+1.5}_{-1.5}$	$10.8^{+1.3}_{-1.2}$	$11.9^{+1.3}_{-1.3}$
h	$0.70^{+0.16}_{-0.15}$	$0.677^{+0.033}_{-0.033}$	$0.709^{+0.017}_{-0.017}$

4 CONCLUSIONS

In this paper we have presented new constraints on the variation of the fine structure constant and on the electron mass using the latest CMB observations, and the full shape of the (spherically averaged) redshift-space correlation function of the CMASS sample of galaxies, drawn from the Data Release 9 (DR9) of the Baryonic Oscillations Spectroscopic Survey (BOSS). Recent BAO and H_0 measurements were also considered. We have studied the degeneracies between these constants and other cosmological parameters, such as the dark energy equation of state, the neutrino mass, the effective number of relativistic species, and the primordial helium abundance. The main results can be summarized as follows:

(i) In the case of variation of only α, our bound is $\alpha/\alpha_0 = 0.9957^{+0.0041}_{-0.0042}$, consistent with no variation at the 2 σ level (almost at 1 σ). The constraints from CMB data alone are slightly improved when CMASS and other cosmological datasets are included.

(ii) When only m_e is allowed to vary, the bounds are highly improved when additional datasets are considered in the analysis. Our best estimate including all datasets is $m_e/(m_e)_0 = 1.006^{+0.014}_{-0.013}$, consistent with no variation of m_e within 1 σ. The CMASS dataset improves largely the CMB-only constraints.

(iii) When both α and m_e are allowed to vary, the constraints on α do not improve with the addition of new datasets, while they do for m_e. With each dataset addition, the variation of the constants becomes more correlated. Our final bounds, using the complete dataset, are $\alpha/\alpha_0 = 0.9901^{+0.0055}_{-0.0054}$ and $m_e/(m_e)_0 = 1.028 \pm 0.019$. Both limits are consistent with no variation of the fundamental constants within 2 σ.

(iv) When we study the variation of α taking the value of $w_{\rm DE}$ as a free parameter, the allowed region for α hardly depends on the addition of further datasets. The constraints on $w_{\rm DE}$, however, are noticeably improved. The bounds for the complete datasets are $\alpha/\alpha_0 = 0.9915 \pm 0.0048$ and $w_{\rm DE} = -1.20 \pm 0.13$, which deviates from the standard value $w_{\rm DE} = -1$ at 1 σ.

(v) When both m_e and $w_{\rm DE}$ are allowed to vary, the CMB dataset cannot place tight constraints on both quantities. The inclusion of CMASS correlation function helps to improve the bounds. Our results for the full dataset are $m_e/(m_e)_0 = 0.996 \pm 0.029$ and $w_{\rm DE} = -1.12 \pm 0.23$.

(vi) When we allow for a non-negligible contribution of massive neutrinos to the dark matter component, our result is $\alpha/\alpha_0 = 0.9978^{+0.0044}_{-0.0045}$, and $f_\nu < 0.043$ at 95% CL for the full dataset. The constraint on the sum of the neutrino masses is $\sum m_\nu < 0.46\,{\rm eV}$ at 95% CL.

(vii) In the case of joint variation of m_e and f_ν, the bounds for the full dataset are $m_e/(m_e)_0 = 1.035 \pm 0.021$, and $f_\nu < 0.086$ at 95% CL. The degeneracies between these quantities and H_0 shift the constraints to higher values when the HST H_0 prior is included.

(viii) When $N_{\rm eff}$ and α are allowed to vary, the values of $N_{\rm eff}$ are consistent within 1 σ with its standard value for the CMB and CMB+CMASS datasets. When the HST H_0 prior is added, the value of $N_{\rm eff}$ is much higher, being slightly consistent at 2 σ with its standard value. The constraint on α is $\alpha/\alpha_0 = 0.9967 \pm 0.0042$, fully consistent with no variation at 1 σ.

(ix) When $N_{\rm eff}$ and m_e are allowed to vary, the value of $N_{\rm eff}$ is more than 1 σ higher than its standard value, and the value of m_e is consistent with no variation at 1 σ, for all of the datasets.

(x) In the case of joint variation of $Y_{\rm He}$ and α, there is a strong degeneracy between these quantities, for all of the datasets. For the CMB and CMB+CMASS datasets, $Y_{\rm He}$ is consistent with the standard value of 0.24. When the H_0 prior is added, $Y_{\rm He}$ is almost 2 σ higher than the standard value. For all of the datasets, there is no variation of α at the 1 σ level.

(xi) In the case of joint variation of $Y_{\rm He}$ and m_e, there is no correlation between these quantities for any dataset. The bounds on $Y_{\rm He}$ are similar for all of the datasets, a value around 2 σ higher than the standard one. For all of the datasets, m_e is consistent with no variation at 1 σ.

(xii) We present new bounds on $N_{\rm eff}$ and $Y_{\rm He}$ in the case of no variation of fundamental constants. For the full dataset, in the ΛCDM+$N_{\rm eff}$ model, the constraint is $N_{\rm eff} = 3.86^{+0.39}_{-0.40}$. In the ΛCDM+$Y_{\rm He}$ model, the constraint is $Y_{\rm He} = 0.301^{+0.028}_{-0.029}$.

The analysis carried out in this paper is based on the first spectroscopic data release of BOSS. Future data releases will provide even more accurate views on the LSS clustering pattern by probing a larger volume of the universe. Together with Planck satellite data to be released in early 2013, this will enable to put more stringent constraints on the variation of fundamental constants.

Table A1. The marginalized 68% allowed regions on the cosmological parameters of the ΛCDM model, obtained using different combinations of the datasets.

	CMB	CMB + CMASS	CMB + CMASS + BAO + H_0
100Θ	$1.0411^{+0.0016}_{-0.0016}$	$1.0407^{+0.0015}_{-0.0015}$	$1.0410^{+0.0015}_{-0.0015}$
$100\omega_{\rm b}$	$2.223^{+0.042}_{-0.042}$	$2.212^{+0.037}_{-0.038}$	$2.223^{+0.038}_{-0.038}$
$100\omega_{\rm dm}$	$11.18^{+0.48}_{-0.48}$	$11.45^{+0.29}_{-0.29}$	$11.45^{+0.21}_{-0.21}$
τ	$0.0850^{+0.0065}_{-0.0068}$	$0.0820^{+0.0057}_{-0.0066}$	$0.0826^{+0.0059}_{-0.0064}$
$n_{\rm s}$	$0.966^{+0.011}_{-0.011}$	$0.9620^{+0.0091}_{-0.0091}$	$0.9641^{+0.0088}_{-0.0087}$
$\ln(10^{10}A_{\rm s})$	$3.081^{+0.030}_{-0.030}$	$3.084^{+0.028}_{-0.028}$	$3.086^{+0.028}_{-0.028}$
$\Omega_{\rm DE}$	$0.733^{+0.025}_{-0.025}$	$0.718^{+0.015}_{-0.015}$	$0.7193^{+0.0099}_{-0.0099}$
$\Omega_{\rm m}$	$0.267^{+0.025}_{-0.025}$	$0.282^{+0.015}_{-0.015}$	$0.2807^{+0.0099}_{-0.0099}$
σ_8	$0.814^{+0.024}_{-0.024}$	$0.825^{+0.018}_{-0.018}$	$0.827^{+0.016}_{-0.016}$
t_0/Gyr	$13.729^{+0.089}_{-0.090}$	$13.769^{+0.071}_{-0.071}$	$13.750^{+0.065}_{-0.064}$
$z_{\rm re}$	$10.4^{+1.2}_{-1.2}$	$10.2^{+1.1}_{-1.2}$	$10.3^{+1.2}_{-1.1}$
h	$0.710^{+0.021}_{-0.021}$	$0.697^{+0.012}_{-0.012}$	$0.6982^{+0.0085}_{-0.0083}$

APPENDIX A: CONSTRAINTS ON THE ΛCDM MODEL

In Table A1, we present our constraints on the cosmological parameters of the ΛCDM model, for better comparison with the results obtained in this paper. These are consistent with the constraints given in Sánchez et al. (2012).

ACKNOWLEDGEMENTS

CGS, JAR-M, RG-S, and RR acknowledge funding from project AYA2010-21766-C03-02 of the Spanish Ministry of Science and Innovation (MICINN). JAR-M is a Ramón y Cajal fellow of the Spanish Ministry of Science and Innovation (MICINN).

Funding for SDSS-III has been provided by the Alfred P. Sloan Foundation, the Participating Institutions, the National Science Foundation, and the U.S. Department of Energy. SDSS-III is managed by the Astrophysical Research Consortium for the Participating Institutions of the SDSS-III Collaboration including the University of Arizona, the Brazilian Participation Group, Brookhaven National Laboratory, University of Cambridge, University of Florida, the French Participation Group, the German Participation Group, the Instituto de Astrofisica de Canarias, the Michigan State/Notre Dame/JINA Participation Group, Johns Hopkins University, Lawrence Berkeley National Laboratory, Max Planck Institute for Astrophysics, Max Planck Institute for Extraterrestrial Physics, New Mexico State University, New York University, Ohio State University, Pennsylvania State University, University of Portsmouth, Princeton University, the Spanish Participation Group, University of Tokyo, University of Utah, Vanderbilt University, University of Virginia, University of Washington, and Yale University.

We acknowledge the use of the Legacy Archive for Microwave Background Data Analysis (LAMBDA). Support for LAMBDA is provided by the NASA Office of Space Science.

REFERENCES

Agafonova, I. I., Molaro, P., Levshakov, S. A., & Hou, J. L. 2011, A&A, 529, A28
SDSS-III Collaboration: Ahn, C., Alexandroff, R., Allende Prieto, C., et al. 2012, arXiv:1207.7137
Aihara, H., Allende Prieto, C., An, D., et al. 2011, ApJS, 193, 29
Alpher, R. A., Bethe, H., & Gamow, G. 1948, Physical Review, 73, 803
Anderson, L., Aubourg, E., Bailey, S., et al. 2012, arXiv:1203.6594
Angulo R. E., Baugh C. M., Frenk C. S., Lacey C. G., 2008, MNRAS, 383, 755
Beutler F., Blake C., Colless M., et al., 2011, MNRAS, 416, 3017
Bize, S., Diddams, S. A., Tanaka, U., et al. 2003, Physical Review Letters, 90, 150802
Blake C., Kazin E. A., Beutler F., et al., 2011, MNRAS, 418, 1707
Bolton, A., et al. 2012, AJ, submitted
Cabré A., Gaztañaga E., 2009, MNRAS, 393, 1183
Chluba, J., & Thomas, R. M. 2011, MNRAS, 412, 748
Coc, A., Descouvemont, P., Olive, K., Uzan, J.-P., & Vangioni, E. 2012, arXiv:1206.1139
Conley A., Guy J., Sullivan M., et al., 2011, ApJS, 192, 1
Crocce M., Scoccimarro R., 2006, PhRvD, 73, 063519
Crocce M., Scoccimarro R., 2008, PhRvD, 77, 023533
Damour, T., & Dyson, F. 1996, Nuclear Physics B, 480, 37
Dawson, K., et al. 2012, AJ, submitted
Dunkley, J., Hlozek, R., Sievers, J., et al. 2011, ApJ, 739, 52
Eisenstein D. J., Hu W., 1998, ApJ, 496, 605
Eisenstein D. J., Seo H.-J., Sirko E., Spergel D. N., 2007, ApJ, 664, 675
Eisenstein D. J., Weinberg D. H., Agol E., et al., 2011, AJ, 142, 72
Fang W., Hu W., Lewis A., 2008, PhRvD, 78, 087303
Fendt, W. A., Chluba, J., Rubiño-Martín, J. A., & Wandelt, B. D. 2009, ApJS, 181, 627
Feng, B., Wang, X., & Zhang, X. 2005, Physics Letters B, 607, 35
Fischer, M., Kolachevsky, N., Zimmermann, M., et al. 2004, Physical Review Letters, 92, 230802
Fujii, Y., Iwamoto, A., Fukahori, T., et al. 2000, Nuclear Physics B, 573, 377
Fukugita, M., Ichikawa, T., Gunn, J. E., et al. 1996, AJ, 111, 1748
García-Berro, E., Isern, J., & Kubyshin, Y. A. 2007, A&AR, 14, 113
Gunn, J. E., Carr, M., Rockosi, C., et al. 1998, AJ, 116, 3040
Gunn, J. E., Siegmund, W. A., Mannery, E. J., et al. 2006, AJ, 131, 2332
Hu, W., & Sugiyama, N. 1996, ApJ, 471, 542
Hu, W. 2005, Phys. Rev. D, 71, 047301
Jones, D. H., Read, M. A., Saunders, W., et al. 2009, MNRAS, 399, 683

Kanekar, N., Langston, G. I., Stocke, J. T., Carilli, C. L., & Menten, K. M. 2012, ApJL, 746, L16
Keisler R., Reichardt C. L., Aird K. A., et al., 2011, ApJ, 743, 28
King, J. A., Webb, J. K., Murphy, M. T., et al. 2012, MNRAS, 422, 3370
Landau, S. J., Mosquera, M. E., Scóccola, C. G., & Vucetich, H. 2008, Phys. Rev. D, 78, 083527
Landau, S. J., & Scóccola, G. 2010, A&A, 517, A62
Larson, D., Dunkley, J., Hinshaw, G., et al. 2011, ApJS, 192, 16
Levshakov, S. A., Combes, F., Boone, F., et al. 2012, A&A, 540, L9
Lewis, A., Challinor, A., & Lasenby, A. 2000, ApJ, 538, 473
Lewis, A., & Bridle, S. 2002, Phys. Rev. D, 66, 103511
Manera, M., Scoccimarro, R., Percival, W. J., et al. 2012, arXiv:1203.6609
Maraston, C. et al. in prep.
Marion, H., Pereira Dos Santos, F., Abgrall, M., et al. 2003, Physical Review Letters, 90, 150801
Matsubara T., 2004, ApJ, 615, 573
Meiksin A., White M., Peacock J. A., 1999, MNRAS, 304, 851
Menegoni, E., Archidiacono, M., Calabrese, E., et al. 2012, Phys. Rev. D, 85, 107301
Montesano F., Sánchez A. G., Phleps S., 2011, arXiv, arXiv:1107.4097
Murphy, M. T., Webb, J. K., & Flambaum, V. V. 2003, MNRAS, 345, 609
Murphy, M. T., Flambaum, V. V., Webb, J. K., & et al. 2004, Astrophysics, Clocks and Fundamental Constants, 648, 131
Olive, K. A., Pospelov, M., Qian, Y.-Z., et al. 2004, Phys. Rev. D, 69, 027701
Padmanabhan N. et al. in prep.
Padmanabhan N., Xu X., Eisenstein D. J., Scalzo R., Cuesta A. J., Mehta K. T., Kazin E., 2012, arXiv, arXiv:1202.0090
Peik, E., Lipphardt, B., Schnatz, H., et al. 2004, Physical Review Letters, 93, 170801
Prestage, J. D., Tjoelker, R. L., & Maleki, L. 1995, Physical Review Letters, 74, 3511
Rahmani, H., Srianand, R., Gupta, N., et al. 2012, arXiv:1206.2653
Reid B. A., Percival W. J., Eisenstein D. J., et al., 2010, MNRAS, 404, 60
Reid, B. A., Samushia, L., White, M., et al. 2012, arXiv:1203.6641
Riess, A. G., Macri, L., Casertano, S., et al. 2011, ApJ, 730, 119
Ross, A. J., Percival, W. J., Sánchez, A. G., et al. 2012, MNRAS, 424, 564
Rubiño-Martín, J. A., Chluba, J., & Sunyaev, R. A. 2008, A&A, 485, 377
Rubiño-Martín, J. A., Chluba, J., Fendt, W. A., & Wandelt, B. D. 2010, MNRAS, 403, 439
Samushia, L., Reid, B. A., White, M., et al. 2012, arXiv:1206.5309
Sánchez A. G., Baugh C. M., Angulo R., 2008, MNRAS, 390, 1470
Sánchez A. G., Crocce M., Cabré A., Baugh C. M., Gaztañaga E., 2009, MNRAS, 400, 1643
Sánchez, A. G., Scóccola, C. G., Ross, A. J., et al. 2012, arXiv:1203.6616
Schramm, D. N., & Turner, M. S. 1998, Reviews of Modern Physics, 70, 303
Scóccola, C. G., Landau, S. J., & Vucetich, H. 2008, Physics Letters B, 669, 212
Seager, S., Sasselov, D. D., & Scott, D. 1999, ApJL, 523, L1
Shaw, J. R., & Chluba, J. 2011, MNRAS, 415, 1343
Smee, S.A., et al. 2012, AJ, submitted
Sortais, Y., Bize, S., & Abgrall, M. 2001, Physica Scripta Volume T, 95, 50
Steigman, G. 2007, Annual Review of Nuclear and Particle Science, 57, 463
Tojeiro, R., Percival, W. J., Wake, D. A., et al. 2012, MNRAS, 424, 136
Uzan, J.-P. 2003, Reviews of Modern Physics, 75, 403
Vikman, A. 2005, Phys. Rev. D, 71, 023515
Webb, J. K., Flambaum, V. V., Churchill, C. W., Drinkwater, M. J., & Barrow, J. D. 1999, Physical Review Letters, 82, 884
Webb, J. K., Murphy, M. T., Flambaum, V. V., et al. 2001, Physical Review Letters, 87, 091301
Webb, J. K., King, J. A., Murphy, M. T., et al. 2011, Physical Review Letters, 107, 191101
Wendt, M., & Molaro, P. 2012, A&A, 541, A69
Wong, W. Y., Moss, A., & Scott, D. 2008, MNRAS, 386, 1023
Xia, J.-Q., Cai, Y.-F., Qiu, T.-T., Zhao, G.-B., & Zhang, X. 2008, International Journal of Modern Physics D, 17, 1229
Xu X., Padmanabhan N., Eisenstein D. J., Mehta K. T., Cuesta A. J., 2012, arXiv, arXiv:1202.0091
York, D.G., et al. 2000, AJ, 120, 1579